DRYOUT DROPLET DISTRIBUTION AND DISPERSED FLOW FILM BOILING

Wayne S. Hill
Warren M. Rohsenow

Report No. 85694-105
Contract No. CME-76-82564 A02

Heat Transfer Laboratory
Department of Mechanical Engineering
Massachusetts Institute of Technology
Cambridge, Massachusetts 02139

August 1982

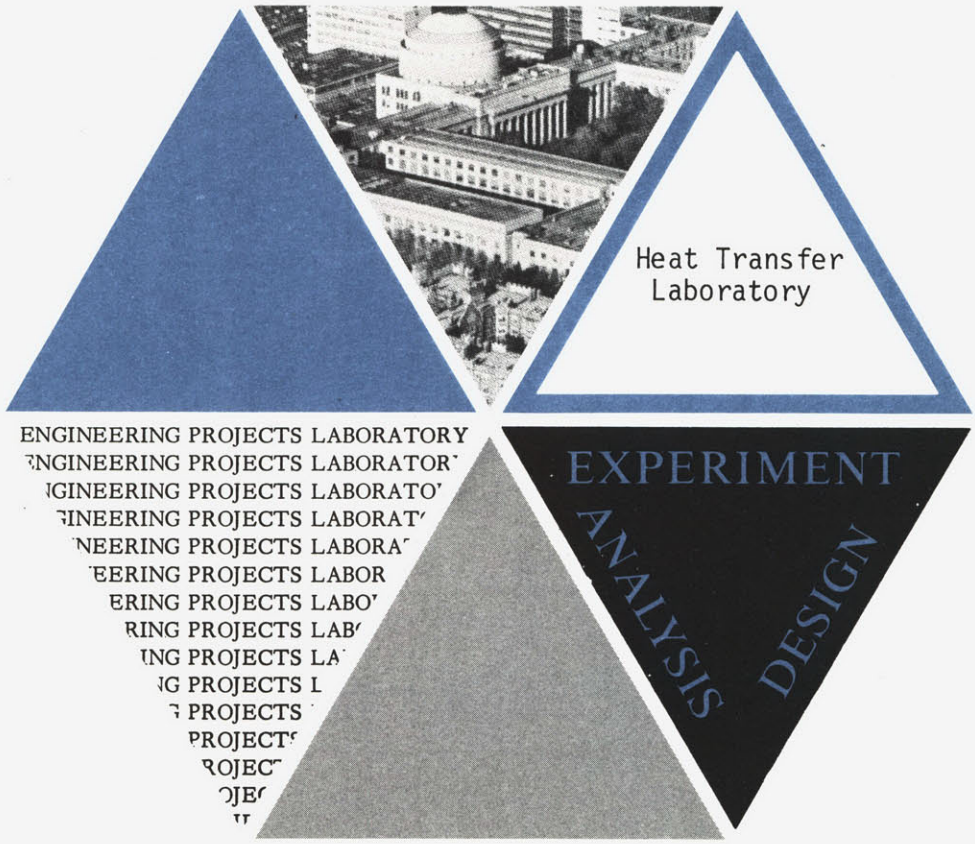

TECHNICAL REPORT No. 85694-105

DRYOUT DROPLET DISTRIBUTION AND DISPERSED FLOW FILM BOILING

by

Wayne S. Hill
Warren M. Rohsenow

Sponsored by
National Science Foundation
Contract No. NSF Grant CME-76=82564 A02
D.S.R. Project No. 85694

August 1982

Department of Mechanical Engineering
Massachusetts Institute of TEchnology
Cambridge, Massachusetts 02139

ABSTRACT

Dispersed flow film boiling is characterized by liquid-phase droplets entrained in a continuous vapor-phase flow. In a previous work at MIT, a model of dispersed flow heat transfer was developed, called the Local Conditions Solution, which is amenable to hand calculation of wall temperatures. This solution identifies a single nonequilibrium parameter which depends solely on conditions at dryout, particularly a characteristic droplet diameter. Previous to the current study, no simple model including mechanisms occurring upstream of dryout had succeeded in predicting the droplet distribution at dryout.

The Local Conditions Solution is rederived to identify which droplet diameter characterizes the distribution of droplets at dryout for purposes of dispersed flow heat transfer analysis. Based on mechanisms of droplet entrainment and deposition, the dryout droplet distribution is derived. This distribution is integrated to obtain the characteristic droplet diameter. A simple method of calculating the characteristic droplet diameter is presented.

With the droplet distribution model, the Local Conditions Solution is compared with three correlations and seven data sets. In general, the Local Conditions Solution predicts wall temperature data to within about 5% better than the three correlations.

It is found that some data display a type of behavior not predicted by the Local Conditions Solution. This may be caused by the enhancement of droplet heat transfer by free stream turbulent fluctuations.

ACKNOWLEDGEMENTS

The authors are grateful to Professors Peter Griffith, Borivoje Mikić, and Ain Sonin for their help and advice. Thanks are also due to Dr. Lawrence Hull for his comments and suggestions. The typing was done by Ms. Gisela Rinner whose assistance is sincerely appreciated.

This research was supported by a grant from the National Science Foundation.

TABLE OF CONTENTS

	Page
Abstract	2
Acknowledgements	3
List of Figures	7
Nomenclature	8
CHAPTER I: INTRODUCTION	12
1.1 Dispersed Flow Heat Transfer	12
1.2 Review of Related Work	18
1.3 Objectives of Research	21
CHAPTER II: BASIC PRINCIPLES OF TWO PHASE FLOWS	23
CHAPTER III: REDERIVATION OF THE LOCAL CONDITIONS SOLUTION	30
3.1 Liquid Mass Balance	30
3.2 Evaporation of Droplets	31
3.3 Flow Heat Balance	32
3.4 Droplet Slip	34
3.5 Drag Coefficient	35
3.6 Droplet Nusselt Number	36
3.7 Nusselt Number Droplet Diameter	37
3.8 Droplet Reynolds Number	39
3.9 Characteristic Droplet Diameter	40
CHAPTER IV: DERIVATION OF DRYOUT DROPLET DISTRIBUTION	42
4.1 Entrained Droplet Diameter	43
4.2 Deposition	48
4.3 Droplet Entrainment Rate	53
4.4 Dryout Droplet Distribution	55
4.5 Characteristic Droplet Diameter	57
4.6 Examination of Assumptions	60
CHAPTER V: APPLICATION TO DISPERSED FLOW FILM BOILING ANALYSIS	65
5.1 Nonequilibrium Parameter	65
5.2 Actual Quality	66
5.3 Vapor Temperature	66
5.4 Wall Temperature	69
5.5 Varying Heat Flux	70
5.6 Core Rod Bundles	72

	Page
CHAPTER VI: COMPARISON WITH OTHER MODELS AND PUBLISHED DATA	74
6.1 Dougall-Rohsenow	74
6.2 Groeneveld and Delorme	75
6.3 Chen et al	76
6.4 Comparison with Data	77
6.5 Summary of Comparisons	90
CHAPTER VII: SUMMARY	91
APPENDICES	94
APPENDIX I: ANNULAR FLOW MODEL	94
APPENDIX II: DRYOUT FILM SLIP RATIO AND RELATIVE VELOCITY	99
APPENDIX III: SAMPLE CALCULATION	102
REFERENCES	108

LIST OF FIGURES

Figure		Page
1-1	Inverted Annular Flow	14
1-2	Annular Flow	15
1-3	Limits of Complete Equilibrium and Complete Nonequilibrium	17
3-1	Comparison of Nusselt Number Correlations	38
4-1	Results of Annular Flow Model for Relative Velocity Between Vapor and Film	46
4-2	Four Regimes of Deposition Velocity	49
4-3	Droplet Deposition Mass Balance	51
4-4	Distribution Factor for $x_b = 0.20$	61
4-5	Distribution Factor Multiplier for Dryout Quality	62
4-6	Mass Distribution vs. Droplet Diameter for $\lambda x_b = 3$, $We_b = 10^5$, and $x_b = 0.5$	63
5-1	Tangent Approximation to Actual Quality vs. Equilibrium Quality, for $K = 0.5$	67
5-2	Actual Quality vs. Equilibrium Quality	68
6-1	Comparison with Bennett et al, Case I	79
6-2	Comparison with Bennett et al, Case II	80
6-3	Comparison with Bennett et al, Case III	82
6-4	Comparison with Bennett et al, Case IV	83
6-5	Comparison with Groeneveld [5]	85
6-6	Comparison with Era et al [3]	86
6-7	Comparison with Hynek [1]	87
A3-1	Actual Quality vs. Equilibrium Quality for Sample Calculation	105

NOMENCLATURE

A	Cross-sectional area (ft^2)
A_c	Dimensionless acceleration group (Eq.(2-9))
B	Mass transport number
C_d	Droplet mass concentration in the core flow (lbm/ft^3)
C_D	Droplet drag cofficient
C_i	Droplet correlation coefficient
C_p	Specific heat at constant pressure (Btu/lbm°R)
$\dot{d}$	Droplet mass deposition rate ($lbm/hr\ ft^2$)
D	Droplet diameter (ft)
D^*	Characteristic droplet diameter (ft)
D_T	Tube diameter (ft)
$\dot{e}$	Mass entrainment rate ($lbm/hr\ ft^2$)
$\dot{E}$	Mass entrained per unit change in quality per unit time (lbm/hr)
f	Distribution factor for $x_b = 0.2$ (Eq. (4-45))
f	Friction factor (Eqs. (A1-5), (A1-6))
F	Distribution factor
g	Gravitational acceleration (ft/hr^2)
G	Mass flux ($lbm/hr\ ft^2$)
Gr	Dimensionless gravity group
h	Heat transfer coefficient ($Btu/hr\ ft^2°R$)
i	Enthalpy (Btu/lbm)

i_{fg}	Heat of vaporization (Btu/lbm)
k	Thermal conductivity (Btu/hr ft°R)
k_d	Deposition velocity (ft/hr)
K	Nonequilibrium parameter (Eqs. (3-23), (5-1))
L	Length (ft)
m	Droplet mass (lbm)
$\dot{n}$	Droplet size distribution ($hr^{-1} ft^{-1}$)
Nu	Nusselt number
p	Pressure (lbf/in^2)
Pr	Prandtl number
q_d	Heat transfer to a droplet (Btu)
$\bar{q}_d$	Average heat transfer rate to a droplet (Btu/hr)
q_w''	Wall heat flux (Btu/hr ft^2)
r_b	Radius of curvature at dryout (Eq. (5-4))
Re	Reynolds number
Re_D'	Reynolds number defined by Eq. (3-18)
Re_b	Dryout Reynolds number (Eq. (4-12))
s	Slip ratio
t	Time (hr)
T	Temperature (°F or °R)
u^*	Friction velocity (Eq. (4-15))
V	Velocity (ft/hr)
w	Mass flow rate (lbm/hr)

We	Weber number
We_b	Dryout Weber number (Eq. (4-11))
x	Quality
z	Axial position (ft)

Greek

α	Void fraction
η	Entrainment fraction
λ	Deposition parameter (Eq. (4-23))
μ	Viscosity (lbm/hr ft)
ρ	Mass density (lbm/ft^3)
σ	Surface tension (lbm/hr^2)
τ	Shear stress (lbf/ft^2)
τ^+	Dimensionless relaxation time (Eq. (4-16))
ϕ	Distribution factor multiplier for dryout quality (Eq. (4-46))
ψ	Nonequilibrium variable of Groeneveld and Delorme [10], (Eq. (6-5))

Subscripts

b	Burnout or dryout
c	Core
crit	Critical

d	Droplet
e	Equilibrium
f	Film
g	Saturated vapor
h	Homogeneous
i	Film-vapor interface
ℓ	Liquid
Nu	Nusselt Number
r	Relative
s	Saturation
ss	Steady State
t	Total
T	Tube
v	Vapor
w	Wall
1	Arithmetic Mean
2	Area Mean
3	Volume Mean

CHAPTER I

INTRODUCTION

1.1 DISPERSED FLOW HEAT TRANSFER

Dispersed flow film boiling is a regime of two phase heat transfer occurring in such applications as once-through steam generators, cryogenic machinery, and in the hypothetical loss-of-coolant accident (LOCA) in nuclear reactors. It is characterized by a dispersion of liquid-phase droplets entrained in a continuous vapor-phase flow.

Because the liquid phase is not in physical contact with the heated wall surface, dispersed flow film boiling can result in high wall temperatures. Even in low pressure steam-water flows, wall temperatures can become high enough for the heated wall material to melt. Consequently, a great deal of effort has been expended in recent years to model dispersed flow heat transfer, particularly for nuclear reactor safety analysis.

Dispersed flow heat transfer can occur in a wide variety of physical geometries, most notably in the complicated geometries of reactor core rod bundles. The most commonly studied geometry for fundamental research, the simplest geometry, is vertical upflow in circular tubes with constant wall heat flux. This is the geometry considered in this study.

Two general types of flow patterns have been observed to pre-

cede the formation of dispersed flow [1]. The wall heat flux and/or the initial wall temperature determines which of these flow regimes occurs.

If the initial wall temperature is high, or the imposed heat flux is very high, inverted annular flow may precede dispersed flow. This pattern is shown in Figure 1-1. In inverted annular flow, the point at which the liquid leaves contact with the wall, the dryout or burnout point, is very near the beginning of the heated section. Wall temperatures are high enough to cause the liquid to form a core in the center of the tube, with a vapor annulus next to the wall. Because of the high density ratio between the liquid and vapor, vapor velocities are much greater than the liquid velocities, and eventually the liquid core becomes unstable. Once the core flow ruptures, droplets are rapidly formed, and dispersed flow is established.

If the inital wall temperature is not very high, or if wall heat fluxes are not very high, annular flow precedes dispersed flow. This pattern is shown in Figure 1-2. As liquid entering the bottom of the tube is heated, vapor bubbles begin to form at the walls. In the nucleate boiling region, liquid remains in contact with the walls, resulting in good heat transfer and low wall temperatures. Because of the low wall temperatures, the liquid and vapor are essentially at saturated conditions. As more vapor is generated, the vapor collects in the center of the tube, surrounded by a liquid film in contact

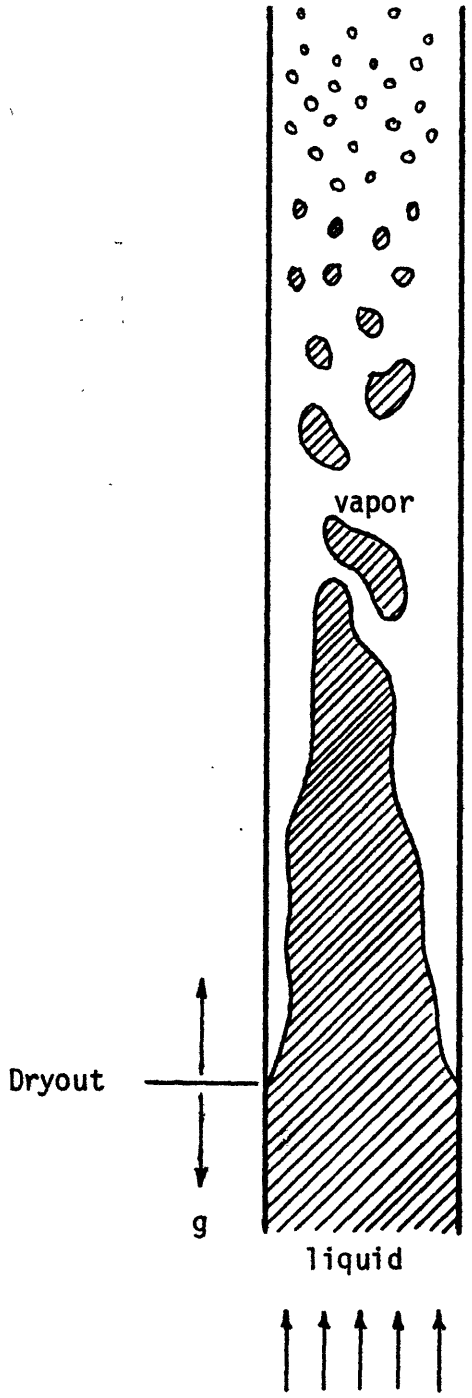

Figure 1-1. Inverted Annular Flow

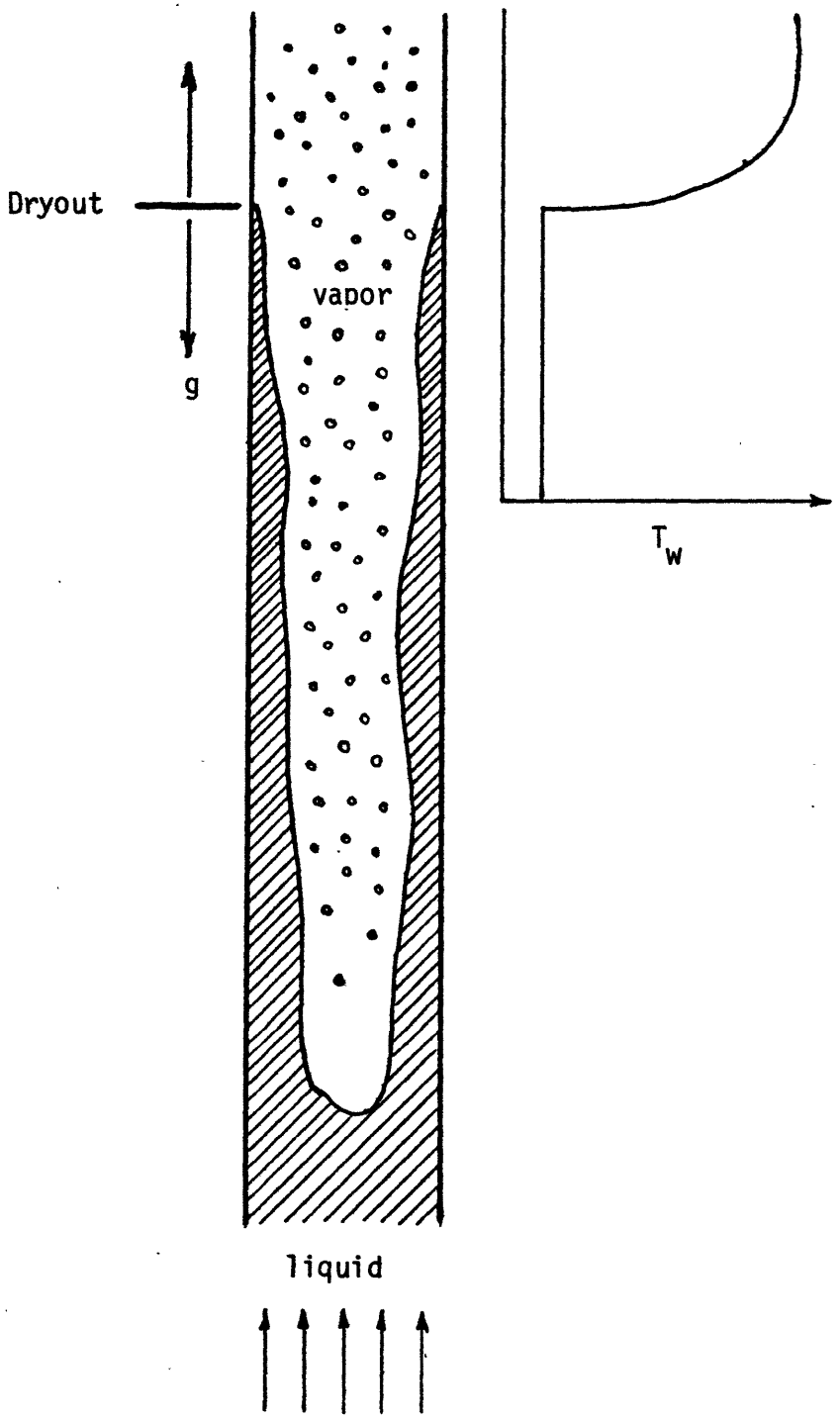

Figure 1-2. Annular Flow

with the wall. The vapor velocities are again much larger than the liquid velocities. Instabilities occurring at the liquid-vapor interface cause droplets to be torn from the film and entrained in the vapor core. Eventually, evaporation and entrainment deplete the liquid film, and dryout or burnout occurs. In this study, it is presumed that annular flow precedes the establishment of dispersed flow.

The most serious complicating factor in the analysis of dispersed flow film boiling is the presence of the liquid droplets in the otherwise continuous vapor flow. Because the liquid is essentially at saturation, while the vapor can be considerably superheated, the droplets behave as a distributed heat sink in the vapor flow. While the droplet volume flow rate is virtually negligible compared to the vapor volume flow rate (void fractions are on the order of .90 to 1.0), the liquid mass flow rate can be comparable to the vapor mass flow rate (dryout qualities can be as low as about .05). Thus, the magnitude of the distributed sink can be considerable. Since most of the heat transferred to the droplets must first be transferred to the vapor, the flow is generally not in complete thermal equilibrium. Thus, the flow is generally somewhere between thermal equilibrium and nonequilibrium, as illustrated qualitatively in Figure 1-3. The degree of thermal nonequilibrium depends on the individual mechanisms that occur in dispersed flow. The analysis becomes even more complicated when the effects of radiation from the wall to the droplets and direct drop-wall interactions are included.

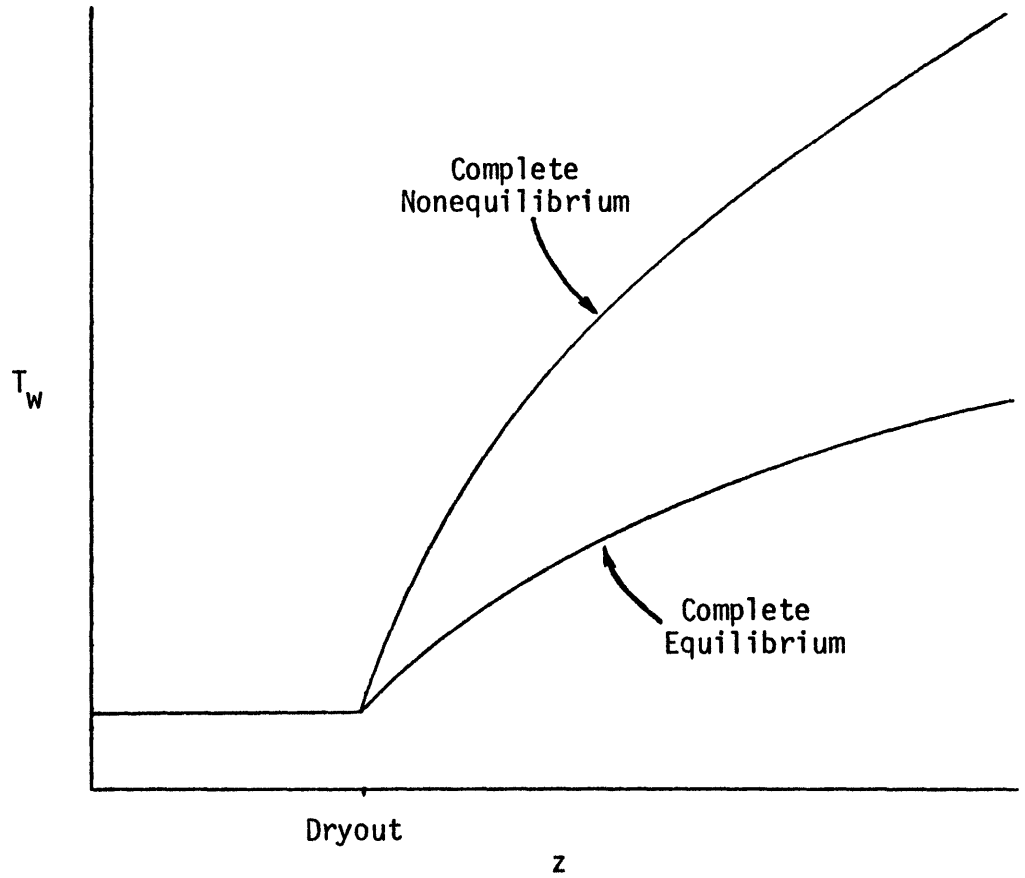

Figure 1-3. Limits of Complete Equilibrium and Complete Nonequilibrium

1.2 REVIEW OF RELATED WORK

EXPERIMENTAL

Experimental data for dispersed flow heat transfer are available for many fluids over a large range of flow conditions and differing physical and flow geometries. Quite a lot of data have been published for vertical circular tubes with constant wall heat flux. Bennet et al [2] and Era et al [3] have taken data using water at 1000 psia. Forslund [4] and Hynek [1] have presented data using nitrogen at low pressures. Groeneveld [5] and Cumo et al [6] have published data using Freon 12, while Koizumi et al [7] used Freon 113.

There are basically two types of approaches which have been utilized in analyzing dispersed flow heat transfer data. These can be divided conveniently into correlative and phenomenological analyses.

CORRELATIVE

Correlations usually begin with an assumption of the general form of the behavior of the flow. Many correlations begin with an accepted equation for pure vapor heat transfer, such as the McAdams or Dittus-Boelter correlation, which is then modified to account for such behaviors as thermal nonequilibrium, droplet slip, and entrance length effects. Free parameters are then evaluated using data from a usually limited number of sources to complete the correlation.

While these solutions are usually simple to apply and are, therefore, attractive, they are generally not valid outside of the data base from which they were developed.

A large number of correlations have been presented in the literature, a partial list of which is presented by Groeneveld and Gardiner [8].

Two correlations which will be considered in this study (see Chapter VI) are those of Chen et al [9] and Groeneveld and Dolorme [10]. Both of these correlations explicitly account for nonequilibrium in the flow, and were developed by back-calculating vapor temperatures from wall temperature data, knowing wall heat flux and assuming a single-phase wall heat transfer coefficient.

PHENOMENOLOGICAL

Most phenomenological models begin with an assumed model of the heat transfer processes occurring in the flow. Using correlations to characterize individual mechanisms, the models follow the flow as it moves down the tube. This usually requires a step by step solution scheme that must be implemented on a computer. The advantage of this approach is that, because specific heat transfer mechanisms are modeled, these models sometimes do better over a wider range of conditions than do correlations.

One of the first of these models, by Dougall [11], (the so-called Dougall-Rohsenow correlation) is simply equivalent to the assump-

tion of thermal equilibrium. Originally, this equation was shown to be an asymptote at high quality for film boiling data at low quality. It was not intended for prediction at low quality. Since this correlation, though not recommended, is still used widely, results of this study are compared with those of Dougall's equation in Chapter VI.

A discussion of the development of phenomenological models of dispersed flow film boiling is presented by Yoder [12]. Yoder created a computer model of dispersed flow heat transfer which included five types of heat transfer interactions. These were: convection from the tube wall to the vapor; convection from the vapor to the droplets; radiation from the wall to the droplets; direct drop-wall interaction; and axial conduction along the tube wall. In general, excellent results were obtained using this model. Yoder found that ignoring radiation, drop-wall interaction, and axial conduction did not result in a serious loss of accuracy of the model's predictions.

This led him to develop a new phenomenological model, based on a two-step heat transfer process. Heat was assumed to be transferred from the wall to the vapor only, and from the vapor to the droplets. This model results in a single differential equation for actual quality vs. equilibrium quality, a measure of thermal nonequilibrium. While this differential equation cannot be analytically integrated, it depends on only one parameter, denoted the nonequlibrium parameter K, which is constant for a given flow situation. Given the conditions at dryout, actual quality could be found as a function of equilibrium

quality, the vapor temperature calculated, and the wall temperature predicted at any position downstream of the dryout location. This model was called the Local Conditions Solution.

The main difficulty of the Local Conditions Solution, and most other phenomenological models of dispersed flow heat transfer, is its dependence on the knowledge of a characteristic droplet diameter at the dryout point. Most researchers simply back-calculate the droplet diameter from other considerations. Yoder's model of the dryout droplet diameter was tedious to apply and initially required numerical experimentation to find an optimal value of a critical Weber number for droplet entrainment.

The purpose of the present study is to develop a phenomenological model of annular flow to predict the characteristic droplet diameter at dryout.

1.3 OBJECTIVES OF RESEARCH

In order to include properly the pertinent physical mechanisms in annular flow which give rise to the droplet distribution at dryout, the phenomenological approach was used in this research. The objectives were as follows:

- To rederive the Local Conditions Solution to determine which droplet diameter is characteristic of the distribution at

dryout for purposes of dispersed flow heat transfer.

- To develop an analytical model based on mass, momentum, and energy conservation equations and recent correlations which describe specific mass transfer mechanisms to predict the droplet distribution at the dryout point.

- To apply this model and appropriate simplifications to the Local Conditions Solution, to result in a simple, accurate model for predicting dispersed flow heat transfer behavior.

- To apply the Local Conditions Solution to published data and to compare the results with those of other correlations.

CHAPTER II

BASIC PRINCIPLES OF TWO PHASE FLOWS

In order to clarify later discussion of the mechanisms occurring in annular and dispersed flows some basic principles and nomenclature of two phase flows are described here.

The total mass flow rate is usually represented by the flow rate per unit cross sectional area, the mass flux.

$$G \equiv \frac{w_t}{A_T} \tag{2-1}$$

The vapor and liquid mass flow rates are sometimes expressed in terms of separate mass fluxes,

$$G_v \equiv \frac{w_t}{A_T} \quad \text{, and} \tag{2-2}$$

$$G_\ell \equiv \frac{w_\ell}{A_T} \quad . \tag{2-3}$$

The vapor and liquid flow rates are related to the total flow rate by the quality (or actual quality).

$$x \equiv \frac{w_v}{w_t} \tag{2-4}$$

$$(1 - x) \equiv \frac{w_\ell}{w_t} \tag{2-5}$$

Thus, the vapor and liquid mass fluxes are

$$G_v = xG \quad , \text{ and} \tag{2-6}$$

$$G_\ell = (1 - x)\, G \, . \tag{2-7}$$

The equilibrium quality x_e is the quality that would occur if the liquid and vapor are in thermodynamic equilibrium. A simple heat balance shows that

$$x_e \equiv \frac{4\, q_w''}{GD_T i_{fg}} (z - z_o) \quad , \tag{2-8}$$

where q_w'' is the wall heat flux (constant), z is the axial position along the tube, and z_o is the location where the enthalpy is the saturated liquid enthalpy, or $x = 0$.

Defining the acceleration group Ac as

$$Ac \equiv \frac{q_w''}{G i_{fg}} \quad , \tag{2-9}$$

results in

$$x_e = \frac{4\,Ac}{D_T}(z - z_o) \quad . \tag{2-10}$$

Because the liquid and vapor are essentially at saturation in annular flow, the actual quality and equilibrium quality are equal in annular flow. However, significant superheating of the vapor can occur in dispersed flow, so the actual and equilibrium qualities are not equal in dispersed flow. It is the prediction of this departure from equilibrium which is the ultimate purpose of this study.

In annular flow, it is often necessary to distinguish between the liquid in the film and the liquid entrained as droplets in the vapor core. This is done using the entrainment fraction

$$\eta \equiv \frac{w_{entrained}}{w_\ell} \quad . \tag{2-11}$$

The fraction of the tube cross section that is covered by vapor is termed the void fraction

$$\alpha \equiv \frac{A_v}{A_T} = \frac{1}{1 + \frac{1-x}{x}\frac{\rho_v}{\rho_\ell} s} \quad , \tag{2-12}$$

where the slip ratio s is the ratio of average vapor and liquid velocities.

$$s \equiv \frac{V_v}{V_\ell} \tag{2-13}$$

In dispersed flow, the slip ratio is an average droplet slip ratio,

$$s_d \equiv \frac{V_v}{V_d} \quad . \tag{2-14}$$

Because $s_d \cong 1$, the void fraction in dispersed flow is approximately the homogeneous void fraction,

$$\alpha \cong \alpha_h \equiv \frac{1}{1 + \frac{1-x}{x}\frac{\rho_v}{\rho_\ell}} \quad . \tag{2-15}$$

Because the liquid in annular flow is distributed between the liquid film and droplets entrained in the core flow, speaking of a single slip ratio in annular flow does not seem to be physically meaningful. Consequently, the core and film void fraction are sometimes differentiated in annular flow. The core void fraction is

$$\alpha_c \equiv \frac{A_v}{A_c} = \frac{1}{1 + \frac{1-x}{x}\eta\frac{\rho_v}{\rho_\ell}s_d} \quad . \tag{2-16}$$

Neglecting the droplet area in the core ($\alpha_c \cong 1$), the film void fraction is approximately

$$\alpha_f \equiv \frac{A_c}{A_T} \cong \frac{1}{1 + \frac{(1-x)(1-\eta)}{x}\frac{\rho_v}{\rho_\ell}s_f} \quad , \tag{2-17}$$

where the film slip ratio is

$$s_f \equiv \frac{V_v}{V_f} \quad . \tag{2-18}$$

It is often necessary to express the vapor velocity or the relative velocities between the vapor and a droplet or the liquid film. The vapor velocity is

$$V_v = \frac{G\,x}{\rho_v \alpha} \quad , \tag{2-19}$$

where $\alpha \cong \alpha_f$ in annular flow, and $\alpha \cong \alpha_h$ in dispersed flow. The relative velocity between the vapor and the liquid film is then

$$V_{rf} = V_v\left(1 - \frac{1}{s_f}\right) \cong \frac{G\,x}{\rho_v \alpha_f}\left(1 - \frac{1}{s_f}\right) \quad , \tag{2-20}$$

and similarly the relative velocity between the vapor and a droplet is

$$V_{rd} = V_v\left(1 - \frac{1}{s_d}\right) \cong \frac{G\,x}{\rho_v \alpha}\left(1 - \frac{1}{s_d}\right) \tag{2-21}$$

Because s_d is near unity, $(1 - \frac{1}{s_d}) \cong (s_d - 1)$. This approximation will prove to be useful later on.

While quality, void fraction, and slip ratio (and entrainment fraction in annular flow) are interrelated, considerations of mass and energy conservation are not sufficient to determine completely the interrelationship. To close the set of equations requires consideration of momentum conservation. In dispersed flow, this comes in the form of a droplet drag coefficient. In annular flow, the situation is further

complicated by separate liquid film and droplet flows. A model has been written for this study based on that of Wallis [13]. In this model, the pressure gradients of the core flow and total flow are modeled separately and equated to yield another relation. With the addition of an assumed entrainment fraction profile, the set of equations is closed. Two versions of the model have been written, one without accelerational effects, and one including accelerational terms, and are described in Appendix I. Unfortunately, neither model yields an explicit analytical result, but requires computer solution.

While the numerical results of both models are of questionable accuracy in describing the phenomena modeled, they do indicate the proper trends, and give some indication of the importance of accelerational effects. In general, the results of both models are quite similar. Film void fractions predicted by both models agree to within one percent, and relative velocities between core and film generally agree to within about six percent. Thus, by and large, accelerational effects can be ignored.

One interesting result is obtained analytically from the non-accelerational model. Near dryout, where both α_f and η approach unity, L'Hopital's rule can be used to obtain the result

$$s_{fb} = \frac{\frac{\rho_\ell}{\rho_v} x_b - 1}{\sqrt{\frac{\rho_\ell}{\rho_v} x_b - 1}} \quad . \tag{2-22}$$

This result, derived in Appendix II, will prove useful in describing the size of entrained droplets later on.

CHAPTER III

REDERIVATION OF THE LOCAL CONDITIONS SOLUTION

The droplets in the core flow are not all of one size: indeed, an entire distribution of droplets is entrained. Until it is known which droplet diameter properly chatacterizes the distribution for purposes of dispersed flow film boiling analysis, the problem description is incomplete.

In order to answer this question, the Local Conditions Solution is derived here including the behavior of a distribution of droplets. Wherever the diameter per se of a droplet is intended, D_1 (the arithmetic mean diameter) is inserted: similarly, whenever the surface area or volume of a droplet is intended, D_2 or D_3 (the surface mean or volume mean diameter) is inserted, respectively. Thus, when the derivation is complete, the characteristic droplet diameter, D^*, will be apparent.

3.1 Liquid Mass Balance

The liquid mass flow rate crossing a plane is

$$w_\ell = \frac{\pi}{6} \dot{n} \rho_\ell D_3^3 = \frac{\pi}{4} D_T^2 G(1 - x) \quad . \tag{3-1}$$

Assuming that no droplets are completely evaporated, the number of drop-

lets crossing a plane per unit time, $\dot{n}$, is constant. From this, it is clear that

$$D_3 = D_{3b}\left(\frac{1 - x}{1 - x_b}\right)^{1/3} \quad . \tag{3-2}$$

Differentiating Equation (3-1),

$$\frac{dw_\ell}{dz} = -\frac{\pi}{4} D_T^2 G \frac{dx}{dz}$$

$$= -\frac{w_\ell}{1-x}\frac{dx}{dz} \quad .$$

From Equation (3-2), then

$$\frac{dw_\ell}{dz} = -\dot{n}\frac{\frac{\pi}{6}\rho_\ell D_{3b}^3}{1 - x}\left(\frac{1 - x}{1 - x_b}\right)^{1/3}\frac{dx}{dz} \quad . \tag{3-3}$$

3.2 Evaporation of Droplets

The time required for a droplet to travel a distance Δz is $\Delta t = \Delta z/V_d$. The heat transferred to a droplet in a distance Δz is thus

$$q_d = \pi D^2 h_d (T_v - T_s)\frac{\Delta z}{V_d} \quad ,$$

so that the mass evaporated from a droplet in traveling a distance Δz is

$$\Delta m_d = - \frac{q_d}{i_{fg}} = - \frac{\pi D^2 h_d (T_v - T_s) \Delta z}{i_{fg} \; V_d} \quad ,$$

Assuming that droplet velocity is independent of diameter, and intergrating over all droplets,

$$\frac{dw_\ell}{dz} = - \dot{n} \frac{\pi D_2^2 h_d (T_v - T_s)}{i_{fg} \; V_d} \quad . \tag{3-4}$$

Equating this to Equation (3-3),

$$\frac{dx}{dz} = 6 \frac{D_2^2}{D_3^2} \frac{h_d (T_v - T_s)}{\rho_\ell i_{fg} V_d} \frac{1 - x}{D_{3b}} \left(\frac{1 - x_b}{1 - x} \right)^{1/3} \quad . \tag{3-5}$$

3.3 Flow Heat Balance

Because some heat goes into superheating the vapor, the actual vapor flow rate is less than that which would occur in an equilibrium situation.

Thus,

$$w_{v_{actual}} = \frac{\pi}{4} D_T^2 G x \quad < \quad w_{v_{equil}} = \frac{\pi}{4} D_T^2 G x_e \quad , \text{ and}$$

$$w_{\ell_{actual}} = \frac{\pi}{4} D_T^2 (1 - x) > w_{\ell_{equil}} = \frac{\pi}{4} D_T^2 G (1 - x_e) \quad .$$

A simple heat balance yields

$$(i_v - i_g)(w_{v_{actual}} - w_{v_{equil}}) = i_{fg} (w_{\ell_{equil}} - w_{\ell_{actual}}) \quad ,$$

or

$$\frac{i_v - i_g}{i_{fg}} = \frac{x_e}{x} - 1 \quad . \tag{3-6}$$

Assuming that $i_v - i_g = C_{pv} (T_v - T_s)$,

$$T_v - T_s = \frac{i_{fg}}{C_{pv}} \left(\frac{x_e}{x} - 1\right) . \tag{3-7}$$

Substituting this into Equation (3-5),

$$\frac{dx}{dz} = 6 \frac{D_2^2}{D_3^2} \frac{h_d}{\rho_\ell C_{pv} V_d} \frac{1 - x}{D_{3b}} \left(\frac{1 - x_b}{1 - x}\right)^{1/3} \left(\frac{x_e}{x} - 1\right) \quad . \tag{3-8}$$

Identifying, from Equation (2-10),

$$dx_e = \frac{4 Ac}{D_T} dz \quad ,$$

and defining

$$h_d \equiv \frac{Nu_d k_v}{D_{Nu}}$$

and

$$V_d \equiv \frac{Re_D' \mu_v}{\rho_v D_T} \quad ,$$

where D_{Nu} is the characteristic droplet diameter for the droplet

Nusselt number,

$$x_e - x = \frac{2}{3}\frac{1}{D_T^2}\frac{D_{3b}D_3^2D_{Nu}}{D_2^2}\frac{1}{(1-x_b)^{1/3}}\,Ac\,Pr_v\,\frac{\rho_\ell}{\rho_v}\frac{Re_D'}{Nu_d}\frac{x}{(1-x)^{2/3}}\frac{dx}{dx_e} \quad . \tag{3-9}$$

3.4 Droplet Slip

Based on a force balance on a droplet, Yoder [12] found

$$\frac{\pi}{6}D^3\rho_\ell V_d\frac{dV_d}{dz} = -\frac{\pi}{6}D^3g(\rho_\ell - \rho_v) + \frac{\pi}{8}D^2C_D\rho_v V_d^2(s_d - 1)^2 \quad ,$$

where C_D is the droplet drag coefficient. Assuming that

$$\frac{dx}{dz} = \frac{dx_e}{dz} \quad ,$$

and

$$x_e\frac{d}{dz}\left(\frac{1}{s_d\alpha}\right) << \frac{1}{\alpha s_d}\frac{dx_e}{dx} \quad ,$$

the following result is obtained.

$$s_d = \frac{1 + \sqrt{1 - \left(1 - \frac{4}{3}\frac{\rho_\ell\rho_v(1-\rho_v/\rho_\ell)g}{G^2C_D}D\frac{\alpha^2}{x^2}\right)\left(1 - \frac{16}{3}Ac\frac{D}{D_T}\frac{\rho_\ell}{\rho_v}\frac{1}{xC_D}\right)}}{\left(1 - \frac{4}{3}\frac{\rho_\ell\rho_v(1-\rho_v/\rho_\ell)g}{G^2C_D}D\frac{\alpha^2}{x^2}\right)} \tag{3-10}$$

Of the previous assumptions, Yoder supports the second rather convincingly. The first assumption is only valid in annular flow. In

dispersed flow, the accuracy depends rather strongly on the degree of departure from thermal equilibrium and will, in some cases, cause significant errors. However, without this assumption, no result could be obtained in closed form. Thus, this model is used in the present work with some reservations.

The effect of gravity is negligible if $\frac{\rho_\ell(\rho_\ell - \rho_v)D\,g}{C_D\,G^2\,x^2} \ll 1.$

This is usually the case except at low qualities. Equation (3-10) then simplifies to

$$s_d \cong 1 + \sqrt{\frac{16}{3}\,\frac{\rho_\ell}{\rho_v}\,Ac\,\frac{1}{x\,C_D}\,\frac{D}{D_T}} \quad . \tag{3-11}$$

The term under the radial is usually small compared to one, so the droplet slip ratio is usually near unity.

3.5 Drag Coefficient

Yoder used the drag coefficient of Ingebo [14] for accelerating spheres,

$$C_D = \frac{27}{Re_d^{.84}} \quad ,$$

with a minimum value of

$$C_{D_{min}} = 0.40 \quad .$$

However, because the accelerations encountered in annular flow are significantly smaller than those in Ingebo's experiments, the hard sphere correlation used by Hynek [1] was used in this study.

$$C_D = \frac{24}{Re_d} (1 + .142\ Re_d^{.698}) \qquad Re_d < 2000 \tag{3-12}$$

3.6 Droplet Nusselt Number

As in Yoder, the droplet Nusselt Number will be characterized by the Ranz and Marshall hard sphere correlation [15],

$$Nu_d = 2 + .6 \left[\frac{\rho_v V_{rd} D}{\mu_{vf}}\right]^{1/2} Pr_{vf}^{1/3} \quad ,$$

modified by Yuen and Chen [16] to account for mass transfer by

$$1 + B = 1 + \frac{C_{pv}(T_v - T_s)}{i_{fg}} \quad ,$$

so that

$$Nu_d = \frac{1}{1 + \frac{C_{pv}(T_v - T_s)}{i_{fg}}} (2 + .6\ Re_{df}^{1/2}\ Pr_{vf}^{1/3}) \tag{3-13}$$

Since the droplet slip ratio is near unity,

$$1 - \frac{1}{s_d} \cong s_d - 1 \cong \sqrt{\frac{16}{3}\frac{\rho_\ell}{\rho_v} Ac \frac{1}{x C_D}\frac{D}{D_T}} \quad ,$$

so

$$V_{rd} \cong \frac{G x}{\rho_v \alpha_h}\sqrt{\frac{16}{3}\frac{\rho_\ell}{\rho_v} Ac \frac{1}{x C_D}\frac{D}{D_T}} \quad . \tag{3-14}$$

It would be convenient if Nu_d could be approximated using a constant drag coefficient, say $C_D = .40$. As shown in Figure 3-1, the Nusselt number is well chararacterized by

$$Nu_d \cong \frac{.63}{1 + \frac{C_{pv}(T_v - T_s)}{i_{fg}}}\left(\frac{G x D}{\mu_{vf}\alpha_h}\sqrt{\frac{16}{3}\frac{\rho_\ell}{\rho_v} Ac \frac{1}{.4 x}\frac{D}{D_T}}\right)^{1/2} Pr_{vf}^{1/3}$$

From Equation (3-7),

$$1 + \frac{C_{pv}(T_v - T_s)}{i_{fg}} = \frac{x_e}{x} \quad ,$$

so

$$Nu_d \cong .63 \frac{x}{x_e}\left(\frac{G x D}{\mu_{vf}\alpha_h}\sqrt{\frac{16}{3}\frac{\rho_\ell}{\rho_v} Ac \frac{1}{.4 x}\frac{D}{D_T}}\right)^{1/2} Pr_{vf}^{1/3} \tag{3-15}$$

3.7 Nusselt Number Droplet Diameter

The Nusselt number droplet diameter is defined so that the heat transfer to a droplet of diameter D_{Nu} is the average heat transfer per droplet. Then

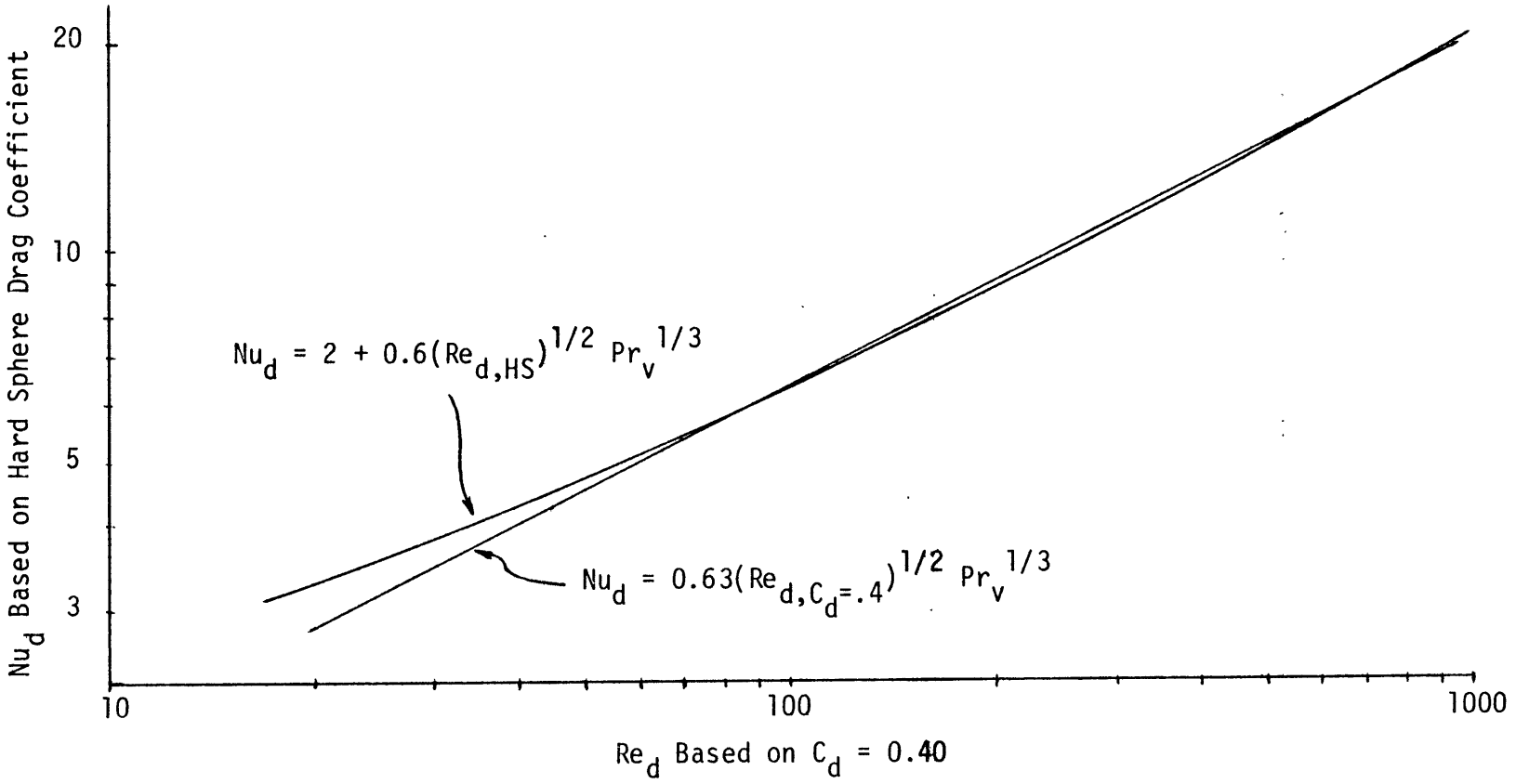

Figure 3-1. Comparison of Nusselt Number Correlations

$$\bar{q}_d = \pi D_{Nu}^2 \frac{Nu_d(D_{Nu})k_v}{D_{Nu}} (T_v - T_s) = \frac{\int_D \pi D^2 \frac{Nu(D)k_v}{D} (T_v - T_s)\, n(D)dD}{\int_D n(D)dD}$$

where $n(D)$ is the droplet size distribution. Since, from Equation (3-15), $Nu_d \sim D^{3/4}$, the above relation suggests that

$$D_{Nu}^{7/4} = \frac{\int_D n(D)D^{7/4}dD}{\int_D n(D)dD} ,$$

or

$$D_{Nu} = D_{7/4} \cong D_2 . \tag{3-16}$$

Since void fraction is close to unity, the variation of void fraction with quality may be neglected. Then, from Equation (3-15),

$$Nu_d \sim \frac{x^{5/4}}{x_e} D_2^{3/4} \tag{3-17}$$

3.8 Droplet Reynolds Number

From the definition of the droplet slip ratio,

$$V_d = \frac{V_v}{s_d} \cong \frac{G\,x}{\rho_v \alpha_h s_d} .$$

Neglecting droplet slip,

$$Re_D' = \frac{G\,x\,D_T}{\mu_v \alpha_h} . \tag{3-18}$$

Again neglecting the variation of void fraction with quality,

$$Re_D' \sim x \quad . \tag{3-19}$$

Equations (3-17) and (3-19) yield

$$\frac{Re_D'}{Nu_d} \cong \frac{x_e}{x^{1/4} x_b^{3/4}} \frac{D_{2b}^{3/4}}{D_2^{3/4}} \frac{Re_{Db}'}{Nu_{db}} \tag{3-20}$$

3.9 Characteristic Droplet Diameter

Sustituting Equations (3-20) into Equation (3-9) results in

$$x_e - x = \frac{2}{3} \frac{1}{D_T} \frac{D_{3b} D_2^{\frac{2}{3}} D_{Nu}}{D_2^2} \frac{D_{2b}^{3/4}}{D_2^{3/4}} \frac{1}{(1-x_b)^{1/3}} Ac\ Pr_v \frac{\rho_\ell}{\rho_v} \frac{Re_{Db}'}{Nu_{db}} \frac{x_e}{x^{1/4} x_b^{3/4} (1-x)^{2/3}} \tag{3-21}$$

Assuming that all droplet diameters vary, like D_3, as $(1 - x)^{1/3}$, Equation (3-21) may be written with $x = x_b = x_e$ at dryout, as follows:

$$K \frac{x^{3/4} x_e}{(1 - x)^{7/12}} \frac{dx}{dx_e} = x_e - x \quad , \tag{3-22}$$

where, evaluating Nu_d at dryout from Equation (3-15), the nonequilibrium parameter is

$$K \cong .554 \left(\frac{D^*}{D_T}\right)^{5/4} \frac{(Ac \frac{\rho_\ell}{\rho_v})^{3/4} Pr_v^{2/3}}{(1 - x_b)^{5/12} x_b^{1/2}} Re_b^{1/2} \quad , \tag{3-23}$$

where the dryout Reynolds number is

$$Re_b \equiv \frac{G x_b D_T}{\mu_v \alpha_b} \quad , \tag{3-24}$$

and where the characteristic droplet diameter is identified to be

$$D^* \equiv \frac{D_3^{12/5}}{D_2^{7/5}} \tag{3-25}$$

Once the characteristic droplet diameter is known, the non-equilibrium parameter can be calculated, and Equation (3-22) can be integrated to yield actual quality as a function of equilibrium quality.

CHAPTER IV

DERIVATION OF DRYOUT DROPLET DISTRIBUTION

Four distinct mechanisms can be identified which could conceivably have an impact on the droplet distribution at dryout. These are:

- Droplet entrainment from the liquid film,
- Coalescence of droplets in the free stream,
- Break-up of droplets in the free stream, and
- Deposition of droplets back onto the liquid film.

Droplet evaporation does not play a part, because the vapor and droplets are essentially saturated upstream of dryout. Because of the high core void fractions common in annular flow (generally > .90) droplet coalescence probably does not occur to a degree great enough to affect substantially the droplet distribution.

The break-up of droplets in the free stream is apparently controlled by a critical Weber number criterion [17],

$$We_{crit} \leq \frac{\rho_v V_{rd}^2 D}{\sigma} \cong \frac{G^2 x^2 D(1 - 1/s_d)^2}{\rho_v \sigma \alpha_f^2} \qquad (4\text{-}1)$$

Since the entrainment of droplets from the liquid film is largely controlled by a Weber number criterion as well (as will be shown in the next section), and the film slip ratio is large compared to the droplet slip ratio, droplets entrained at one point travel a long distance before break-up. From Eq. (4-1),

$$\frac{x_{\text{break-up}}}{x_{\text{entrain}}} \sim \frac{1 - \frac{1}{s_f}}{1 - \frac{1}{s_d}} \quad . \tag{4-2}$$

Consequently, if any droplet break-up occurs at all, it is the large droplets that were initially entrained (many of which have already been redeposited) that break up first. Thus, for now, break-up will be ignored, an assumption to be reexamined later.

Thus, the mechanisms that are considered here are the entrainment of droplets from the liquid film to the vapor core and the deposition of droplets back onto the liquid film.

4.1 ENTRAINED DROPLET DIAMETER

While several mechanisms of droplet entrainment have been identified (e.g., wave undercutting, droplet impingement, and liquid bridge disintegration), it is generally believed that the shearing off of roll wave tops is the predominant mechanism occurring in annular flow. Kataoka, et al. [18] expressed the distribution of droplets entrained at a point (translated into the current nomenclature) as a modified Weber number criterion.

$$D_i = C_i \frac{\sigma \rho_v}{G^2 x^2} \left(\frac{G \times D_T}{\mu_v} \right)^{2/3} \left(\frac{\rho_\ell}{\rho_v} \right)^{1/3} \left(\frac{\mu_v}{\mu_\ell} \right)^{2/3} , \tag{4-3}$$

where

$$C_1 = .0031 \quad \text{for} \quad D_1 \quad , \tag{4-4}$$

$$C_2 = .0040 \quad \text{for} \quad D_2 \quad , \text{ and} \tag{4-5}$$

$$C_3 = .0053 \quad \text{for} \quad D_3 \quad . \tag{4-6}$$

This correlation was developed from adiabatic air-water data, where the large density ratio results in void fractions near unity and very large film slip ratios, and consequently

$$V_{rf} = \frac{Gx}{\rho_v \alpha}\left(1 - \frac{1}{s_f}\right) \cong \frac{Gx}{\rho_v} \quad . \tag{4-7}$$

Because the area of application of this study is largely in high pressure applications, where smaller density ratios result in smaller void fractions and film slip ratios, this relative velocity effect requires further investigation.

Yoder used Ahmad's slip ratio [19] to characterize film slip.

$$s_f = \left(\frac{\rho_\ell}{\rho_v}\right)^{.205} \left(\frac{G\, D_T}{\mu_\ell}\right)^{-.016}$$

However, this slip ratio was derived from void fraction data at low qualities. Because void fraction is quite insensitive to slip ratio, but slip ratio is sensitive to void fraction, the application of this correlation to relative velocity estimation is of questionable validity.

Instead, for this study, an analytical result from the void fraction model, derived in Appendix II, will be used. The dryout film slip ratio is

$$s_{fb} = \frac{\left(\frac{\rho_\ell}{\rho_v} x_b - 1\right)}{\sqrt{\frac{\rho_\ell}{\rho_v} x_b - 1}} \quad ,$$

or

$$V_{rfb} = \frac{G\,x_b}{\rho_v}\left(1 - \frac{1}{s_{fb}}\right) = \frac{G\,x_b}{\rho_v}\,\frac{\sqrt{\frac{\rho_\ell}{\rho_v}\,x_b}}{\sqrt{\frac{\rho_\ell}{\rho_v}\,x_b} + 1} \quad . \tag{4-8}$$

In Figure 4-1, V_{rf}/V_{rfb} is plotted against x/x_b for two cases of practical interest. These data are results of the annular flow model with no acceleration. As is apparent from the figure, V_{rf}/V_{rfb} is not a strong function of the gravity group,

$$Gr = \frac{\rho_\ell \rho_v g\, D_T}{G^2} \quad .$$

Picking an average case, a curve fit yields

$$\frac{V_{rf}}{V_{rfb}} \cong (x/x_b)^{1+1.23(x/x_b)^2} \quad . \tag{4-9}$$

For high pressure applications, Eq. (4-3) is modified by replacing $V_{rf}^2 \cong (Gx/\rho_v)^2$ with V_{rf}^2 found from Eqs. (4-8) and (4-9). This leaves

$$D_i = C_i \frac{\sigma \rho_v}{G^2 x_b^2}\left(\frac{GxD_T}{\mu_v}\right)^{2/3}\left(\frac{\rho_\ell}{\rho_v}\right)^{1/3}\left(\frac{\mu_v}{\mu_\ell}\right)^{2/3}$$

$$\frac{\left(\sqrt{\frac{\rho_\ell}{\rho_v}\,x_b} + 1\right)^2}{\frac{\rho_\ell}{\rho_v}\,x_b}\left(\frac{x}{x_b}\right)^{-(2+2.46(x/x_b)^2)} \quad ,$$

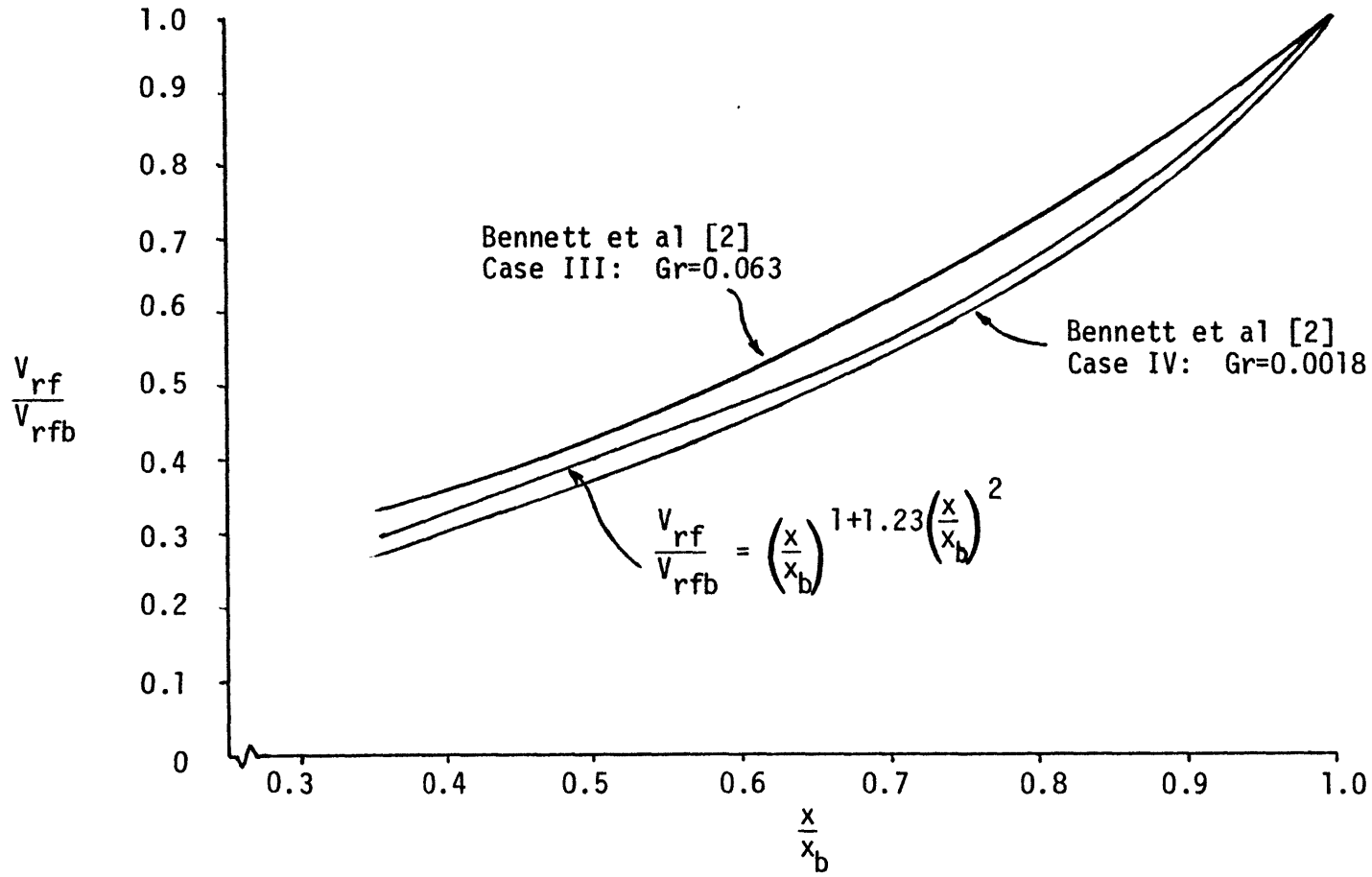

Figure 4-1. Results of Annular Flow Model for Relative Velocity Between Vapor and Film

or

$$\frac{D_i}{D_T} = \frac{C_i}{We_b} (Re_b)^{2/3} \left(\frac{\rho_\ell}{\rho_v} \right)^{1/3} \left(\frac{\mu_v}{\mu_\ell} \right)^{2/3} \frac{\left(\sqrt{\frac{\rho_\ell}{\rho_v} x_b} + 1 \right)^2}{\frac{\rho_\ell}{\rho_v} x_b} \left(\frac{x}{x_b} \right)^{-(4/3 + 2.46(x/x_b)^2)} , \tag{4-10}$$

where the dryout Weber number is

$$We_b \equiv \frac{G^2 x_b^2 D_T}{\rho_v \sigma} , \tag{4-11}$$

and the dryout Reynolds number is

$$Re_b \equiv \frac{G x_b D_T}{\mu_v} . \tag{4-12}$$

One reassuring feature of this droplet correlation is that, because, from Eqs. (4-10), (4-11) and (4-12),

$$\frac{D}{D_T} \sim \frac{1}{D_T^{1/3}} ,$$

it is unlikely that a droplet diameter will be predicted to be larger than the tube diameter, thus averting a preposterous limiting behavior.

Consideration of the rate at which entrainment occurs will be delayed until after droplet deposition is considered.

4.2 DEPOSITION

Droplet deposition is usually characterized by a deposition velocity k_d.

$$\dot{d} = k_d C_d \quad , \tag{4-13}$$

where $\dot{d}$ is the mass deposited per unit film area per unit time, and C_d is the droplet mass concentration in the core flow,

$$C_d = \frac{\text{Entrained Mass Flow Rate}}{\text{Core Area} \cdot \text{Droplet Velocity}}$$

$$= \frac{\frac{\pi}{6} \rho_\ell D^3 \dot{n}}{\frac{\pi}{4} D_T^2 \alpha_f V_d} = \frac{2}{3} \frac{\rho_\ell D^3 \dot{n}}{D_T^2 \alpha_f V_d} \quad , \tag{4-14}$$

where $\dot{n}$ is the number of droplets crossing a plane per unit time. McCoy and Hanratty [20] identified four regimes of deposition velocity, Figure 4-2. In the graph, u^* is the friction velocity,

$$u^{*2} = .03955 \frac{(Gx)^{7/4} \mu_v^{1/4}}{\rho_v^2 D_T^{1/4}} \quad , \tag{4-15}$$

and τ^+ is the dimensionless relaxation time

$$\tau^+ = \frac{D^2 \rho_v \rho_\ell u^{*2}}{18 \mu_v^2} = 2.20 \times 10^{-3} \frac{\rho_\ell D^2 (Gx)^{7/4}}{\rho_v D_T^{1/4} \mu_v^{7/4}} \quad . \tag{4-16}$$

The first regime is controlled by Brownian motion, and thus occurs only in submicron particles. The second regime also occurs only in small

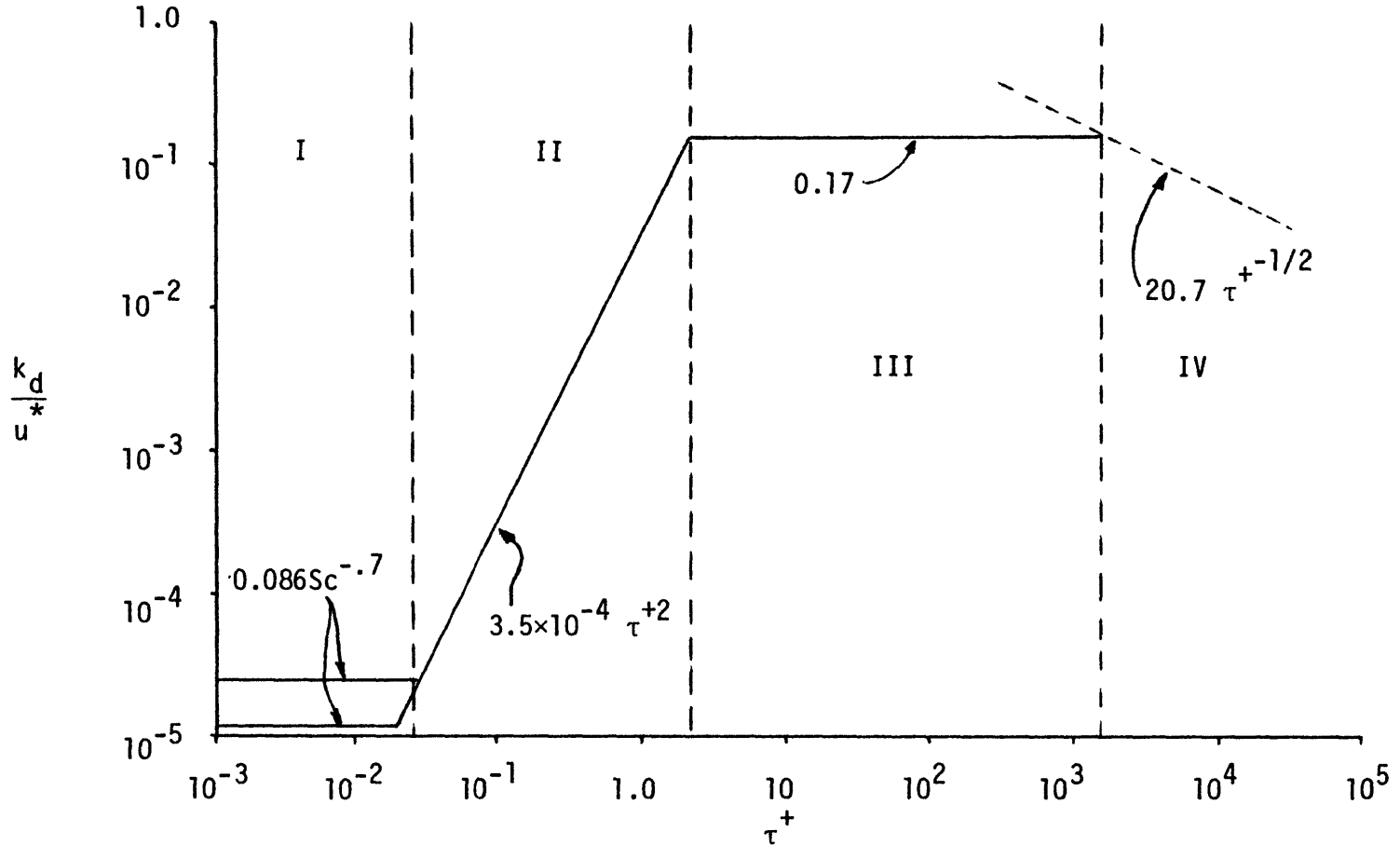

Figure 4-2. Four Regimes of Deposition Velocity

particles or in low speed flows. In fact, results of the annular flow model described in Appendix I indicate that only the third and fourth regimes occur in annular flow, and the third regime appears to be strongly predominant.

Thus, it is assumed for purposes of this study that only the third regime occurs, so that $k_d/u^* = 0.17$, or with Eq. (4-15)

$$k_d = .0338 \frac{(Gx)^{7/8} \mu_v^{1/8}}{\rho_v D_T^{1/8}} \quad . \tag{4-17}$$

Assuming that the core void fraction $\alpha_c \cong 1$, and neglecting droplet slip,

$$V_d = \frac{Gx}{\rho_v \alpha_f} \quad , \tag{4-18}$$

so the droplet deposition rate, from Eqs. (4-13), (4-14), (4-17), and (4-18), is

$$\dot{d} \cong \frac{2}{3} \frac{.0338}{\left(\frac{GxD_T}{\mu_v} \right)^{1/8}} \frac{\rho_\ell D^3 \dot{n}}{D_T^2} \quad . \tag{4-19}$$

Consider the deposition of a packet of droplets of diameter D traveling in the core flow, Figure 4-3. A mass balance gives

$$\frac{d\dot{n}}{dx} = -\frac{3}{2} \frac{D_T^2 \dot{d} \sqrt{\alpha_f}}{D^3 \rho_\ell Ac} = -\frac{.0338 \sqrt{\alpha_f} \dot{n}}{\left(\frac{GxD_T}{\mu_v} \right)^{1/8} Ac} \quad . \tag{4-20}$$

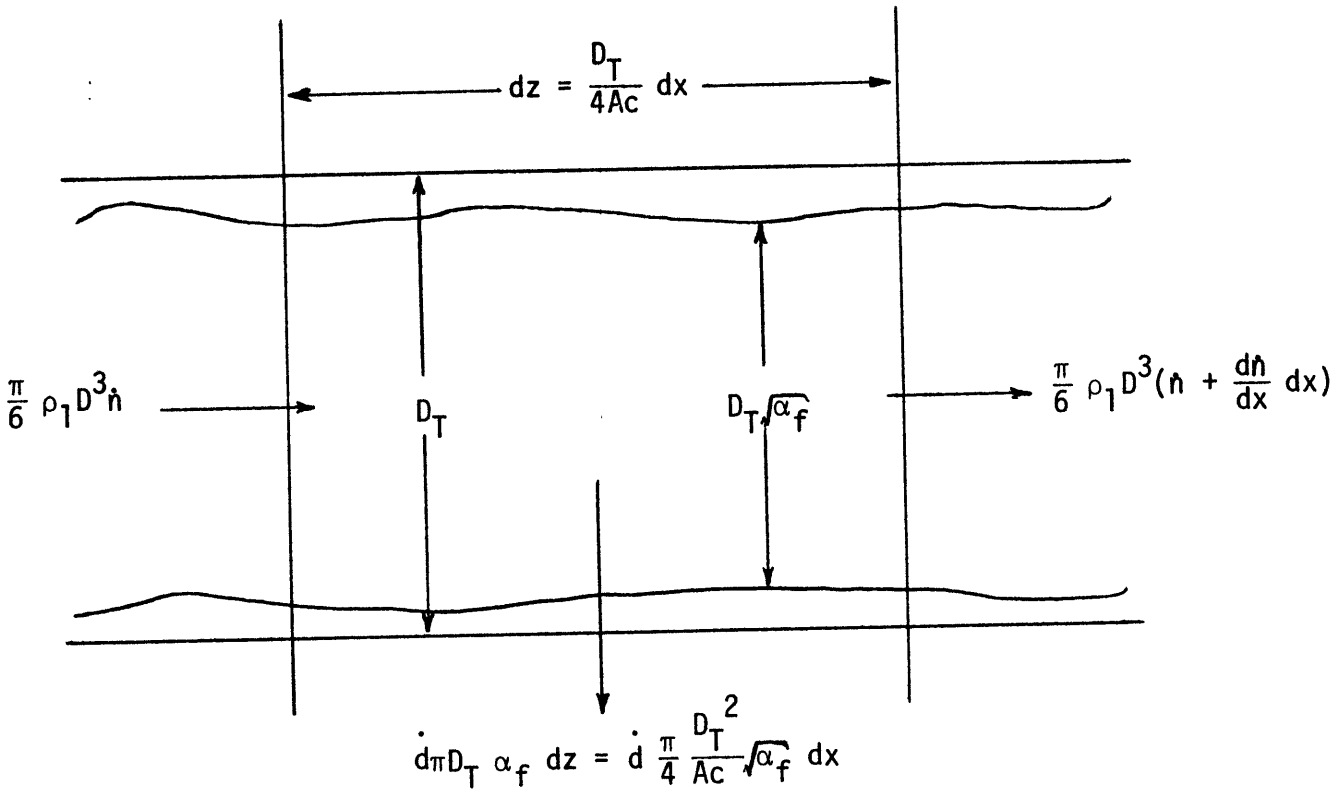

Figure 4-3. Droplet Deposition Mass Balance

Thus, the number deposition rate is independent of droplet diameter. Assuming the film void fraction can be approximated by

$$\alpha_f \cong \left(\frac{x}{x_b}\right)^{1/4} \tag{4-21}$$

(an assumption not inconsistent with the results of the annular flow model),

$$\frac{d\dot{n}}{dx} = - \frac{.0338\ \dot{n}}{\left(\frac{G\ x_b D_T}{\mu_v}\right)^{1/8} Ac} = - \lambda \dot{n} \quad . \tag{4-22}$$

where the deposition parameter is

$$\lambda \equiv \frac{.0338}{\left(\frac{G\ x_b D_T}{\mu_v}\right)^{1/8} Ac} \quad . \tag{4-23}$$

Since the number deposition rate is independent of droplet diameter, the average droplet diameter of a distribution of droplets initially entrained at some initial quality x_i is the same as the average of those droplets surviving to some later quality x_f . Thus, it is not necessary to keep track of the changing shape of a distribution of droplets entrained at a given point. Instead, a distribution entrained at a point can be characterized by an average diameter $D(x)$ and a number $\dot{n}(D)$. By integrating Eq. (4-22),

$$\dot{n}(D) = \dot{n}_e(D) e^{-\lambda(x-x_i)} \quad , \tag{4-24}$$

where $\dot{n}_e(D)$ is the number flow rate of droplets entrained at x_i, and $\dot{n}(D)$ is the number flow rate of droplets entrained at x_i that survive to x.

It now only remains to characterize the droplet entrainment rate, before the droplet distribution at dryout is determined.

4.3 DROPLET ENTRAINMENT RATE

Because it cannot be measured directly, droplet entrainment rate can only be inferred from entrainment fraction and deposition rate measurements at steady state in an adiabatic flow. In this case entrainment and deposition rates must be equal,

$$\dot{e}_{ss} = \dot{d}_{ss} = k_d C_{dss} \quad , \tag{4-25}$$

where $\dot{e}$ is the mass entrainment rate per unit film area per unit time. In terms of flow variables, with Eq. (4-18),

$$C_{dss} = \frac{\frac{\pi}{4} D_T^2 G(1-x)\eta_{ss}}{\frac{\pi}{6} D_T^2 \alpha_f V_d} \cong \rho_v \frac{(1-x)}{x} \eta_{ss} \quad , \tag{4-26}$$

where droplet slip ratio s_d is assumed unity, and where η_{ss} is the steady state entrainment fraction. Assuming that the entrainment and deposition mechanisms are independent,

$$\dot{e} = k_d C_{dss} \tag{4-27}$$

in general, not just at steady state conditions. Recalling from Eq. (4-17) that

$$k_d = .0338 \frac{(Gx)^{7/8} \mu_v^{1/8}}{\rho_v D_T^{1/8}}$$

results in

$$\dot{e} = \frac{.0338 (Gx)^{7/8} \mu_v^{1/8}}{D_T^{1/8}} \frac{1-x}{x} \eta_{ss} \quad . \tag{4-28}$$

The mass entrained per unit change in quality per unit time,

$$\dot{E} = \dot{e}(\text{film circumference})\left(\frac{dz}{dx}\right)$$

$$= \dot{e}(\pi D_T \sqrt{\alpha_f})\left(\frac{D_T}{4Ac}\right) \quad . \tag{4-29}$$

As in Eq. (4-21), assuming that $\alpha_f \cong \left(\frac{x}{x_b}\right)^{1/4}$, this results in

$$\dot{E} = \frac{\pi}{4} D_T^2 G(1-x)\lambda\eta_{ss} \quad , \tag{4-30}$$

where λ is defined in Eq. (4-23). Some characterization of η_{ss} is still needed.

Ishii and Mishima [21] correlated η_{ss} as

$$\eta_{ss} = \tanh\left(7.25\times10^{-7}\left(\frac{G^2x^2D_T}{\rho_v\sigma}\left(\frac{\rho_\ell - \rho_v}{\rho_v}\right)^{1/3}\right)^{5/4}\right.$$
$$\left.\left(\frac{G(1-x)D_T}{\mu_\ell}\right)^{1/4}\right) \quad . \tag{4-31}$$

This correlation was based on air-water data at low pressure, but results in unreasonably low values of η_{ss} at higher pressures. The data of Cousins and Hewitt [22], upon which the correlation was based in part, indicate that for large enough liquid Reynolds numbers, η_{ss} is independent of Reynolds number; therefore, the data of Cousins and Hewitt were reevaluated to produce an alternative entrainment fraction correlation,

$$\eta_{ss} = (1 - e^{-.01935\ Re_\ell^{.6306}}) \tanh(5.341\times10^{-5}\ We^{1.277}) \qquad (4\text{-}32)$$

Equations (4-31) and (4-32) both agree well with the data. In most cases in annular flow, liquid Reynolds numbers are large enough that they have no effect on η_{ss}. Combining Eqs. (4-30) and (4-32) for the case where $\exp(-0.01935\ Re_\ell^{0.6306}) \ll 1$,

$$\dot{E} \cong \frac{\pi}{4} D_T^2 G(1-x)\lambda \tanh\left(5.341\times10^{-5} \left(\frac{G^2x^2D_T}{\rho_v\sigma}\right)^{1.277}\right) . \qquad (4\text{-}33)$$

4.4 DRYOUT DROPLET DISTRIBUTION

Determining the droplet distribution at dryout is now a relatively simple problem. The number flow rate of droplets entrained between x and $x+\Delta x$ is

$$\dot{n} = \frac{\dot{E}}{\frac{\pi}{6}\rho_\ell D(x)^3} , \qquad (4\text{-}34)$$

where $D(x)$ is found from Eq. (4-10). The number flow rate of droplets of size between $D(x)$ and $D(x) + \Delta D$ entrained at x is then

$$\dot{n} = - \frac{\dot{E}}{\frac{\pi}{6} \rho_\ell D(x)^3 \frac{dD(x)}{dx}} \quad , \tag{4-35}$$

where the minus sign appears because $\frac{dD(x)}{dx}$ is negative. From Eq. (4-24), then, the number flow rate of droplets between D and $D + \Delta D$ surviving to dryout is

$$\dot{n}(D) = - \frac{\dot{E}}{\frac{\pi}{6} \rho_\ell D(x)^3 \left. \frac{dD(x)}{dx} \right|_{x(D)}} e^{-\lambda(x_b - x(D))} \quad , \tag{4-36}$$

where $x(D)$ is the quality at which droplets of diameter D are entrained. Substituting Eq. (4-33) for $\dot{E}$ yields the dryout droplet distribution,

$$\dot{n}(D) = - \frac{3}{2} \frac{D_T^2 G}{\rho_\ell D(x)^3 \left. \frac{dD(x)}{dx} \right|_{x(D)}} (1-x)_{x(D)} \lambda \tanh(5.341 \times 10^{-5} \left(\frac{G^2 x^2 D_T}{\rho_v \sigma} \right)^{1.277}_{x(D)}) e^{-\lambda(x_b - x(D))} \tag{4-37}$$

where

$$D_i(x) = \frac{C_i D_T}{We_b} Re_b^{2/3} \left(\frac{\rho_\ell}{\rho_v} \right)^{1/3} \left(\frac{\mu_v}{\mu_\ell} \right)^{2/3} \frac{\left(\sqrt{\frac{\rho_\ell}{\rho_v}} x_b + 1 \right)^2}{\frac{\rho_\ell}{\rho_v} x_b} \left(\frac{x}{x_b} \right)^{-(4/3 + 2.46(x/x_b)^2)} \quad , \tag{4-10}$$

where

$$C_1 = .0031 \quad \text{for} \quad D_1 \quad ,$$

$$C_2 = .0040 \quad \text{for} \quad D_2 \quad , \quad \text{and}$$

$$C_3 = .0053 \quad \text{for} \quad D_3 \quad .$$

4.5 CHARACTERISTIC DROPLET DIAMETER

Recall from Eq. (3-25) that the characteristic droplet diameter was identified as

$$D^* = \frac{D_3^{12/5}}{D_2^{7/5}} \quad .$$

This can be represented with Eq. (4-10), as

$$\frac{D^*}{D_T} = \frac{(F)^{4/5}\ .00786}{We_b} (Re_b)^{2/3} \left(\frac{\rho_\ell}{\rho_v}\right)^{1/3} \left(\frac{\mu_v}{\mu_\ell}\right)^{2/3} \frac{\left(\sqrt{\frac{\rho_\ell}{\rho_v}}\, x_b + 1\right)^2}{\frac{\rho_\ell}{\rho_v}\, x_b} \quad , \qquad (4\text{-}38)$$

where the constant

$$.00786 = \frac{C_3^{12/5}}{C_2^{7/5}} \qquad (4\text{-}39)$$

and

$$F^{4/5} \equiv \left(\frac{x^*}{x_b}\right)^{-(4/3 + 2.46(x^*/x_b)^2)} \quad , \qquad (4\text{-}40)$$

where x^* is the quality at which D^* is entrained, and where the distribution factor F takes into account the shape of the dryout droplet distribution. The volume and surface mean diameters are defined by

$$D_3 \equiv \left[\frac{\int_D^{} \dot{n}(D) D^3 dD}{\int_D^{} \dot{n}(D)\, dD} \right]^{1/3} , \tag{4-41}$$

and

$$D_2 \cong \sqrt{\frac{\int_D^{} \dot{n}(D) D^2 dD}{\int_D^{} \dot{n}(D)\, dD}} . \tag{4-42}$$

Equations (4-41) and (4-42) are evaluated using $\dot{n}(D)$ from Eq. (4-37) and $D_i(x)$ and $dD(x)/dx$ from Eq. (4-10). Substituting this result into Eq. (3-25) to find D^*, and solving Eq. (4-38) for the distribution factor F results in Eq. (4-43) on the next page. None of the integrals required to calculate F can be solved analytically, so numerical integration is required. Because the distribution factor is a function of three independent variables, an infinite number of graphs would normally be needed to represent F completely. As it turns out, however, F can be approximated with only a few percent error as

$$F^{4/5} = \frac{\left[\int_0^1 \left(\frac{1}{x_b} - \frac{x}{x_b}\right)\lambda x_b \tanh\left(5.341\times10^{-5}(We_b)^{1.277}\left(\frac{x}{x_b}\right)^{1.277}\right) e^{-\lambda x_b\left(1-\frac{x}{x_b}\right)} d\left(\frac{x}{x_b}\right)\right]^{4/5}}{\left[\int_0^1 \frac{\left(\frac{1}{x_b} - \frac{x}{x_b}\right)\lambda x_b}{\left[\left(\frac{x}{x_b}\right)^{-(4/3+2.46(x/x_b)^2)}\right]^3} \tanh\left(5.341\times10^{-5}\, We_b^{1.277}\right)\left(\frac{x}{x_b}\right)^{1.277} e^{-\lambda x_b\left(1-\frac{x}{x_b}\right)} d\left(\frac{x}{x_b}\right)\right]^{7/10}}$$

$$\frac{\left[\int_0^1 \frac{\left(\frac{1}{x_b} - \frac{x}{x_b}\right)\lambda x_b}{\left(\frac{x}{x_b}\right)^{-(4/3+2.46(x/x_b)^2)}} \tanh\left(5.341\times10^{-5}\, We_b^{1.277}\left(\frac{x}{x_b}\right)^{1.277}\right) e^{-\lambda x_b\left(1-\frac{x}{x_b}\right)} d\left(\frac{x}{x_b}\right)\right]}{\left[\int_0^1 \frac{\left(\frac{1}{x_b} - \frac{x}{x_b}\right)\lambda x_b}{\left[\left(\frac{x}{x_b}\right)\right]^3} \tanh\left(5.341\times10^{-5}\, We_b^{1.277}\left(\frac{x}{x_b}\right)^{1.277}\right) e^{-\lambda x_b\left(1-\frac{x}{x_b}\right)} d\left(\frac{x}{x_b}\right)\right]} \quad (4\text{-}43)$$

$$= F^{4/5}(We_b, \lambda x_b, x_b)$$

$$F \cong \phi(We_b, x_b)\, f(We_b, \lambda x_b) \tag{4-44}$$

where

$$f = F(We_b, \lambda x_b, \text{ at } x_b = 0.2) \tag{4-45}$$

$$\phi = \frac{F(We_b, \lambda x_b, x_b)}{F(We_b, \lambda x_b, \text{ at } x_b = 0.2)} \tag{4-46}$$

The functions f and ϕ are plotted in Figures 4-4 and 4-5. Thus, using Figures 4-4 and 4-5 and Eq. (4-38), the characteristic droplet diameter can be calculated relatively simply.

4.6 EXAMINATION OF ASSUMPTIONS

In Figure 4-6, the mass distribution $\dot{n}D$ is plotted against D/D_b for the case $\lambda x_b = 3$, $x_b = .5$, $We_b = 10^5$. As is clear from the figure, large droplets account for a very small percentage of the droplet mass flow. Numerical experimentation shows that droplets entrained before $x/x_b = .5$ have little effect on D^*. Thus, unless such a large amount of droplet break-up occurs that a droplet of diameter D^* is in danger of breaking up at dryout, droplet break-up can be ignored altogether. In none of the cases investigated in Chapter VI did a droplet of diameter D^* suffer a free stream Weber number large enough that it was in danger of breaking up (assuming, after Yoder [12], that $We_{crit} = 6.5$).

In Figure 4-4, it is apparent that f is relatively insensitive to λx_b. Consequently, the assumptions required to characterize droplet

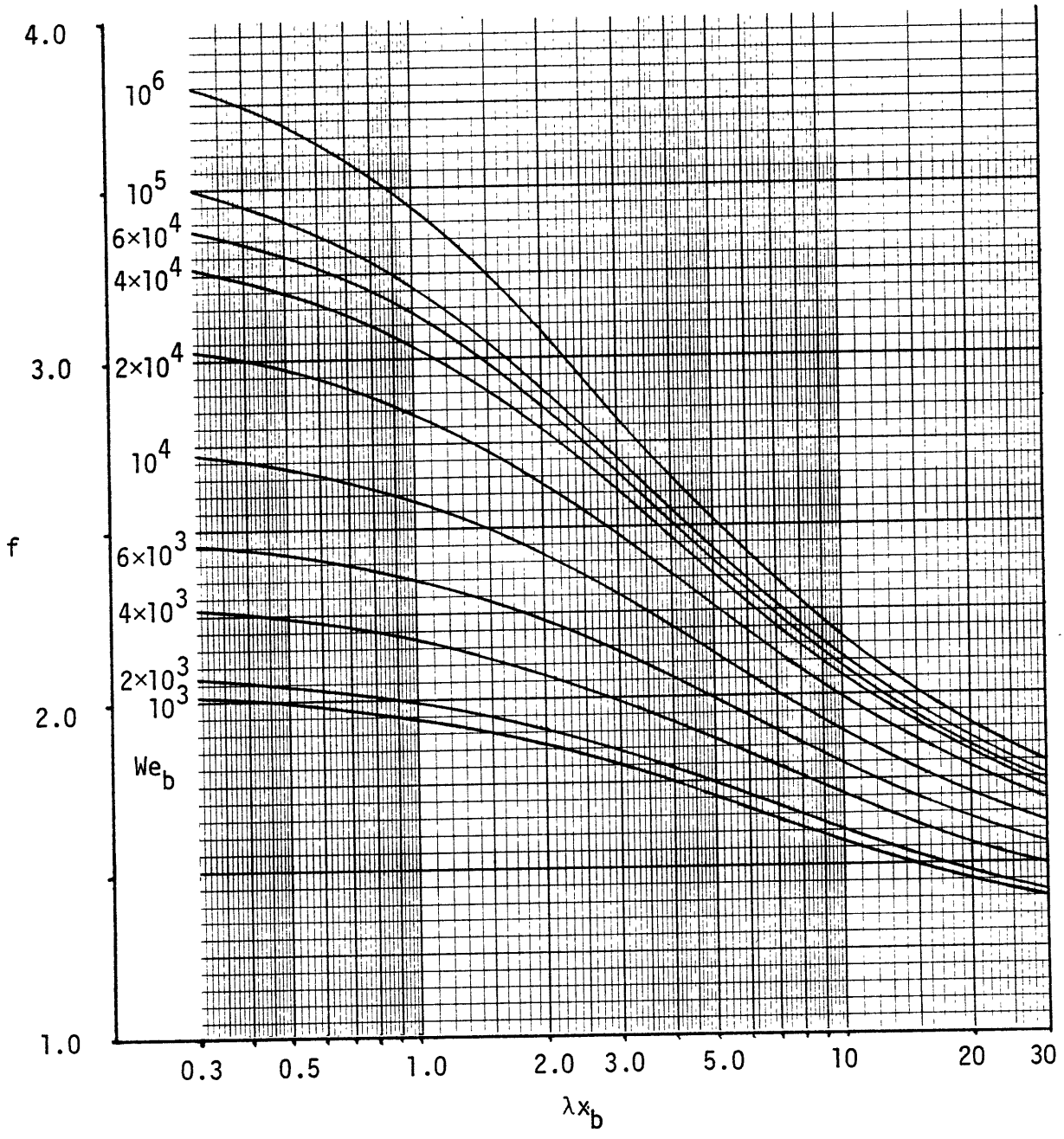

Figure 4-4. Distribution Factor for $x_b = 0.20$

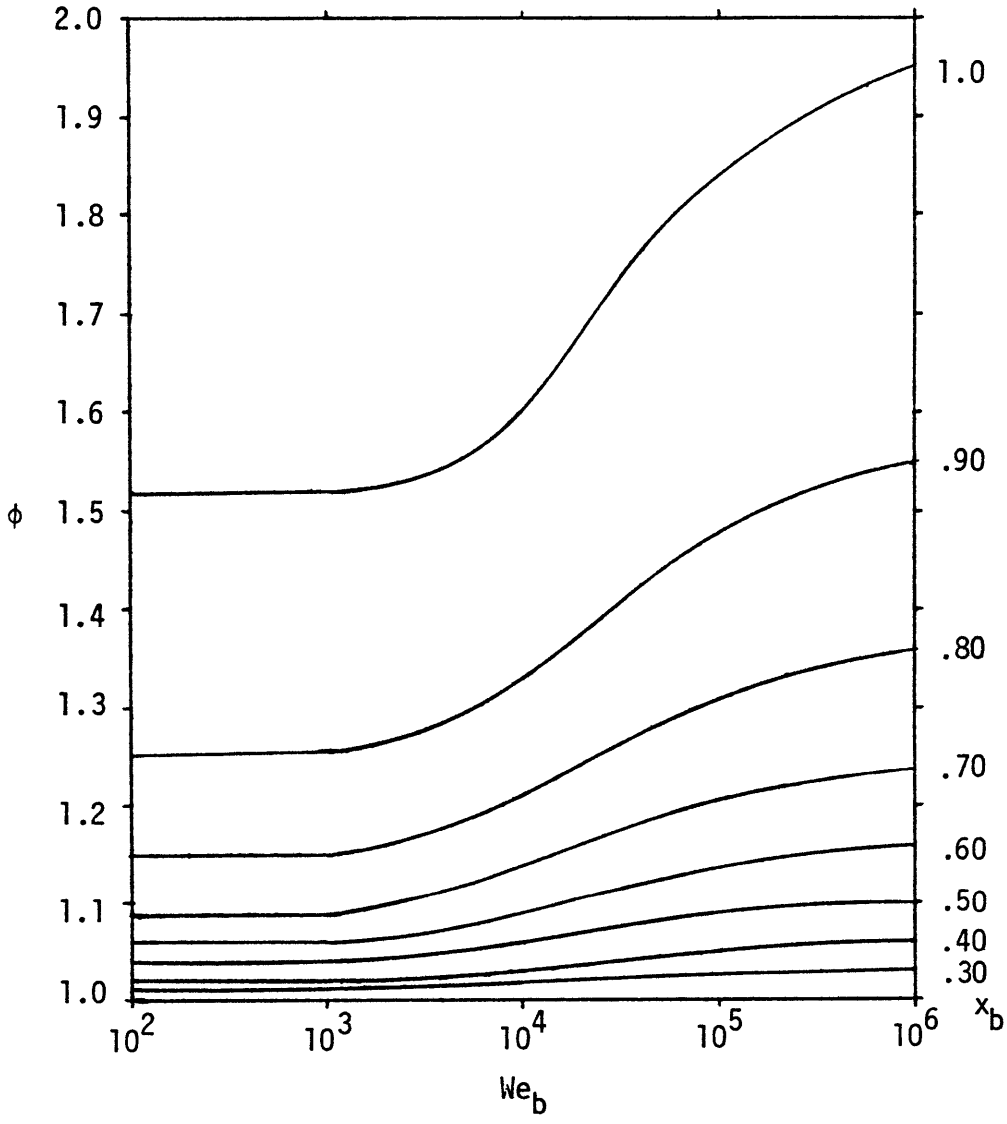

Figure 4-5. Distribution Factor Multiplier for Dryout Quality

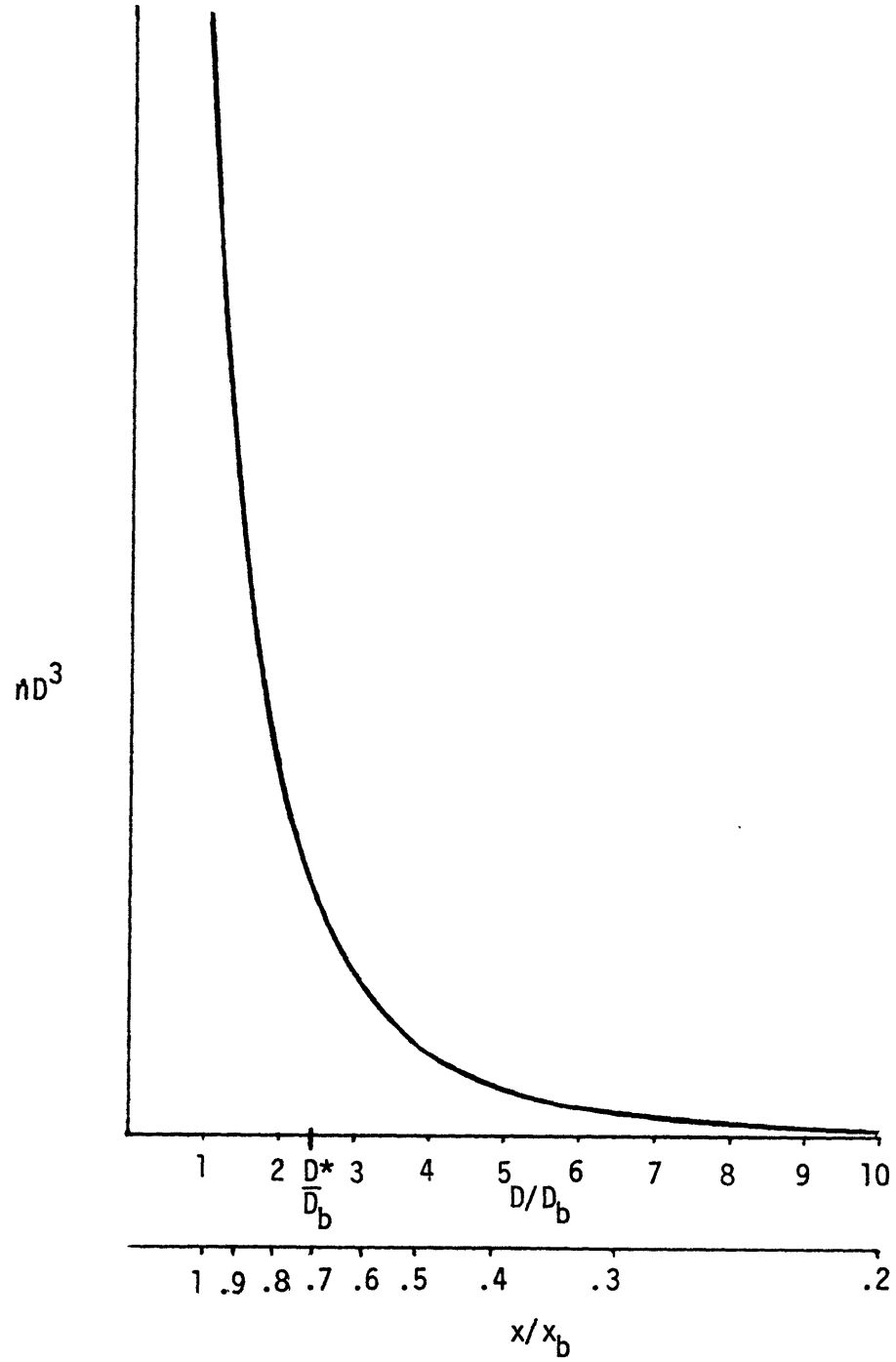

Figure 4-6. Mass Distribution vs. Droplet Diameter for $\lambda x_b=3$, $We_b=10^5$, and $x_b=0.5$

deposition (namely, $\alpha_f \cong (x/x_b)^{1/4}$, $s_d \cong 1$, and deposition is characterized by the third regime only) are justified.

It is not really possible to determine the accuracy of either the entrained droplet size correlation or the entrainment rate characterization. While Cumo, et al. [23] and Ueda [24] have performed experiments to measure entrained droplet diameters, the accuracy of these measurements is inherently poor, and insufficient information was given to compare their results with those predicted here. Consequently, the only method available for verification of this model is comparison of results of the Local Conditions Solution with published heat transfer data.

CHAPTER V

APPLICATION TO DISPERSED FLOW HEAT TRANSFER ANALYSIS

5.1 NONEQUILIBRIUM PARAMETER

From Eq. (3-22),

$$K \frac{x^{3/4}\, x_e}{(1-x)^{7/12}} \frac{dx}{dx_e} = x_e - x \quad , \tag{3-22}$$

where Eq. (3-23) gives

$$K \cong .554 \left(\frac{D^*}{D_T} \right)^{5/4} \frac{\left(Ac \frac{\rho_\ell}{\rho_v}\right)^{3/4} Pr_v^{2/3}}{(1-x_b)^{5/12}\, x_b^{1/2}} (Re_b)^{1/2} \quad . \tag{3-23}$$

Introducing D^*/D_T from Eq. (4-38) yields

$$K \cong .0013 \frac{f\phi Ac^{3/4} Pr_v^{2/3} Re_b^{4/3} \left(\sqrt{\frac{\rho_\ell}{\rho_v}}\, x_b + 1\right)^{5/2}}{We_b^{5/4} (1-x_b)^{5/2} x_b^{7/4} \left(\frac{\rho_\ell}{\rho_v}\right)^{1/12}} \left(\frac{\mu_v}{\mu_\ell}\right)^{5/6} \quad , \tag{5-1}$$

where f and ϕ are found from Figures 4-4 and 4-5,

$$A_c \equiv \frac{q''_w}{G\, i_{fg}} \quad ,$$

$$Re_b \equiv \frac{G\, x_b\, D_T}{\mu_v \alpha_h} = \frac{G\, D_T}{\mu_v} \left(x_b + \frac{\rho_v}{\rho_\ell} (1 - x_b)\right)$$

$$We_b \equiv \frac{G^2 x_b^2 D_T}{\rho_v \sigma}$$

$$\lambda x_b = \frac{.0338\ x_b}{(Re_b)^{1/8} Ac} \tag{5-2}$$

5.2 ACTUAL QUALITY

Equation (3-22) is integrated from $x_b = x = x_e$ for a given value of K. In general, x is a function of three independent variables, x_b, K, and x_e, so that an infinite number of graphs should be required to represent all cases of the integral. Differentiating Eq. (3-22) with $dx/dx_e = 0$ at dryout yields the radius of curvature of x vs. x_e near dryout,

$$r_b = \frac{K\ x_b^{7/4}}{(1-x_b)^{7/12}} \quad . \tag{5-3}$$

As shown in Figure 5-1, for a given value of K, solutions for all values of x_b approach one another for large values of x_e. Thus, at a given dryout quality, an arc of radius r_b can be constructed. A line tangent to this arc and to the solution for $x_b = .1$ is a good approximation to the exact integral. Thus, the integrals in Figure 5-2, with $x_b = .1$ and many values of K, are all that is needed to accurately predict actual quality from K, x_b, and equilibrium quality.

5.3 VAPOR TEMPERATURE

Once x is known as a function of x_e, the vapor temperature is

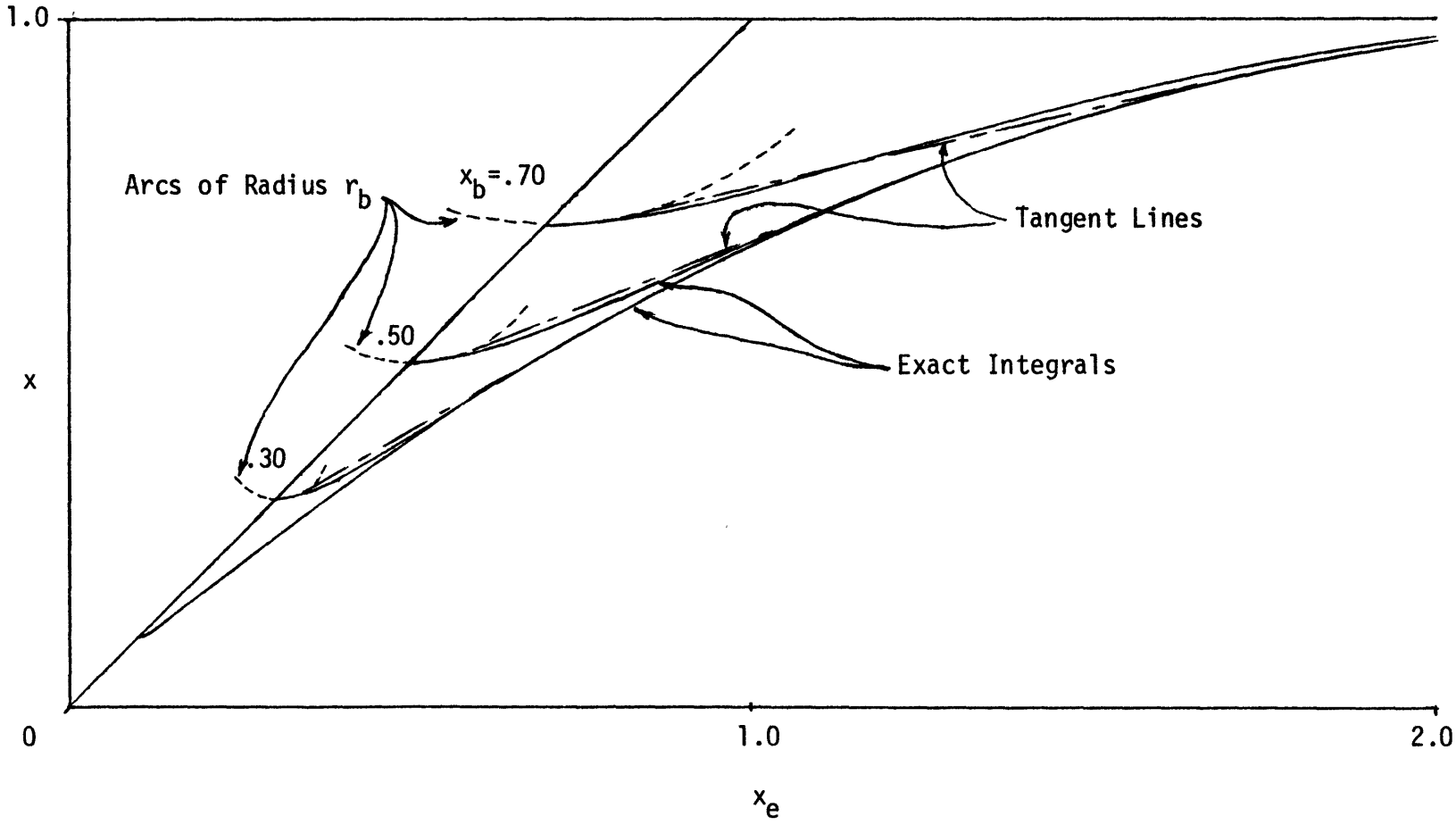

Figure 5-1. Tangent Approximation to Actual Quality vs. Equilibrium Quality, for K=0.5

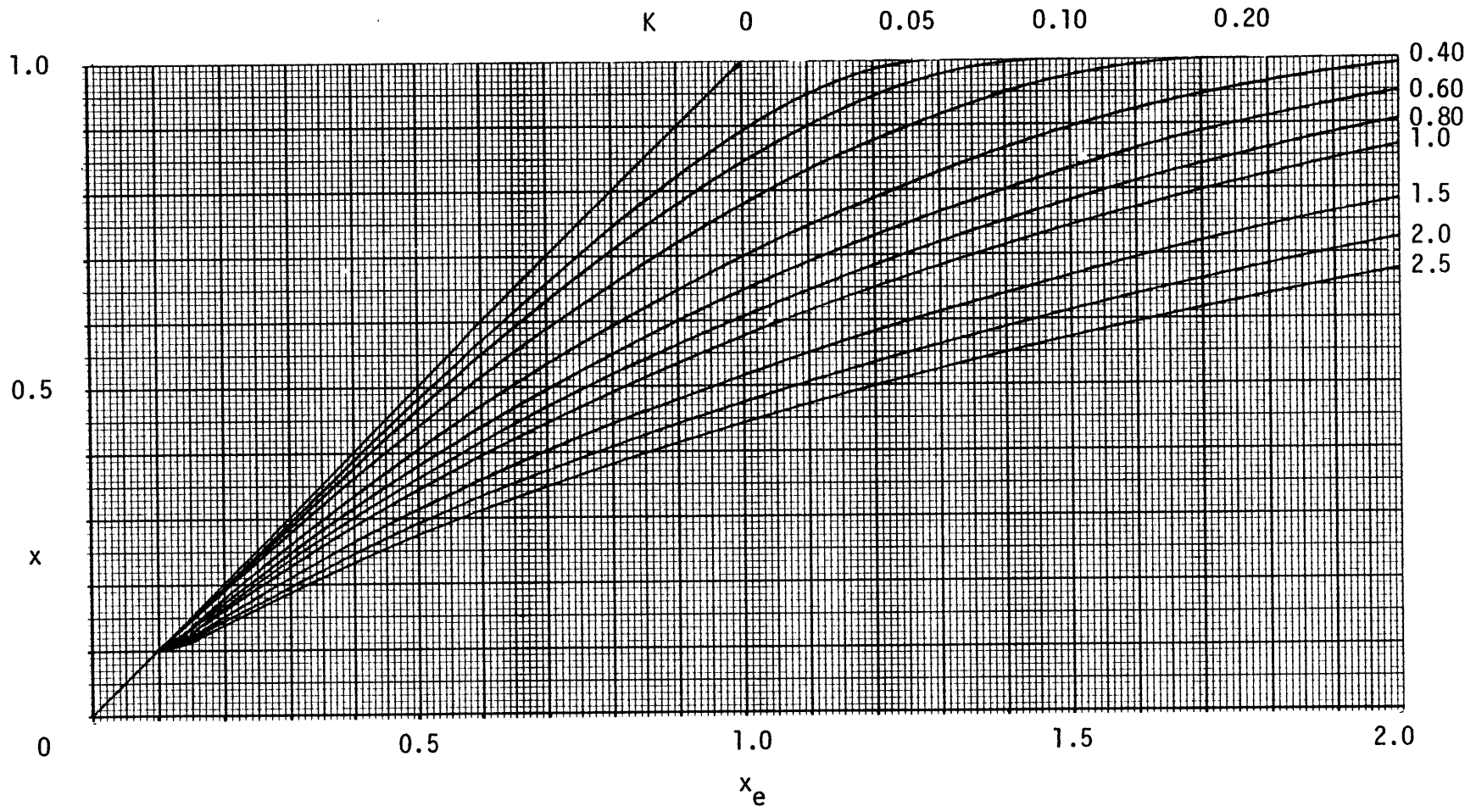

Figure 5-2. Actual Quality vs. Equilibrium Quality

found from Eq. (3-6),

$$\frac{i_v - i_g}{i_{fg}} = \frac{x_e}{x} - 1 \quad . \tag{5-4}$$

5.4 WALL TEMPERATURE

Knowing the vapor temperature, tube wall temperature is found from

$$T_w - T_v = \frac{q''_w}{h_w} \quad , \tag{5-5}$$

where h_w is the vapor single phase heat transfer coefficient. Following the lead of Groeneveld and Delorme [10], Hadaller's heat transfer coefficient [21] is used,

$$h_w = .008348 \frac{k_{vf}}{D_T} Pr_f^{.6112} \left(\frac{G \times D_T}{\mu_{vf} \alpha_h} \right)^{.8774} \quad , \tag{5-6}$$

where the subscript f indicates evaluation of a property at the film temperature, $T_f = \frac{1}{2}(T_v + T_w)$. Because it is assumed that q''_w is known, but T_w is not, some iteration is usually required to obtain T_w .

Just downstream of dryout, the presence of liquid droplets in the vapor flow suppresses the development of the thermal boundary layer. Consequently, a single phase entrance length correlation will underestimate the wall heat transfer coefficient, so no entrance length correlation was used in this work. In another work on the M.I.T. Dispersed

Flow Project, Hull [25] has developed a model of the effect of droplets on the thermal boundary layer growth.

In Appendix III, one of the cases presented in the next chapter is worked out in a sample calculation.

5.5 VARYING HEAT FLUX

The current model is not strictly applicable to cases where the wall heat flux is not constant, because the acceleration group

$$Ac = \frac{q''_w}{G\, i_{fg}}$$

is assumed constant in calculating the nonequilibrium parameter K . In problems of practical interest, though, wall heat flux generally varies both with position and time, so some means of modifying the model for these cases is necessary.

VARIATION WITH POSITION

Upstream of dryout, variation of heat flux with position will only affect the analysis by way of its effect on the deposition parameter λx_b , Eq. (5-2). Since the characteristic droplet diameter is relatively insensitive to λx_b (Figure 4-4), the analysis will usually be affected only by very strongly varying wall fluxes. In cases where the wall flux varies by as much as a factor of two between $x_e = 0$ and dryout, the average heat flux between $x/x_b = .75$ and $x/x_b = 1$ should be used to calculate λx_b . Inspection of Figure 4-6 suggests that the droplets entrained in this region contribute most to the determination of the characteristic droplet diameter.

Downstream of dryout, variation of heat flux with position results in a nonequilibrium parameter that is a function of position. Generally, an error in K of 10% results in relatively minor errors in predicted wall temperature, so errors in average wall flux of 15% are acceptable. When wall heat flux varies strongly with position, the problem should be broken up into sections wherein q''_w varies by 30%, and K calculated for each section based on x_b and average wall heat flux. Equation (3-22) should then be integrated from section to section to calculate actual quality and vapor temperature, and the local wall heat flux used to calculate wall temperature.

VARIATION WITH TIME

Once annular flow has developed, the time required for the dryout droplet distribution to react to a change in heat flux is characterized by the time required for a droplet entrained at $x = \frac{1}{2} x_b$ to travel to the dryout point. This is roughly

$$\Delta t_1 \sim \frac{L}{V_d} \sim \frac{\frac{x_b D_T}{4Ac}}{\frac{G x_b}{2 \rho_v}} \sim \frac{\rho_v i_{fg} D_T}{q''_w} \quad .$$

As long as this time is short compared to a time characteristic of the variation in wall flux, the droplet model can be used without modification.

Downstream of dryout, the time required for the flow to react to a change in heat flux depends upon the length downstream that is of interest,

$$\Delta t_2 \sim \frac{L}{V_v} \sim \frac{L \rho_v}{G} \quad ,$$

where L is the length of interest. As long as $\Delta t_1 + \Delta t_2$ is small compared to the characteristic time for variation in wall flux (which should be true even in a rapid reflood problem) the Local Conditions Solution can be used without modification, except to use the actual wall heat flux as a function of time in calculating λx_b and K.

In cases where wall heat flux varies more rapidly than $\Delta t_1 + \Delta t_2$, the current model should not be used without modifications for transient analysis.

5.6 CORE ROD BUNDLES

Analysis of dispersed flow film boiling in nuclear reactor rod bundles is of great importance in reactor safety analysis. While the current model is not directly applicable to this geometry, it could possibly be made to do a creditable job with some modifications.

Assuming that secondary flow phenomena within the bundle can be ignored, the tube diameter D_T of the current model can simply be replaced by the hydraulic diameter of a rod cell. The effect of grid spacers on the droplet distribution is, however, more complicated.

A fraction of the droplets entrained in the vapor flow strikes a grid spacer. This fraction is roughly the ratio of the spacer area to the total flow area. The liquid is then re-entrained as droplets whose size is determined by a critical Weber number criterion,

$$We_c = \frac{G^2 x^2 D}{\rho_v \sigma} \quad .$$

Thus, the characteristic droplet diameter downstream of a grid spacer is different from that upstream of a spacer.

The best way to model a rod bundle with grid spacers would thus involve recalculating K from Eq. (3-23) at each grid spacer based on a new characteristic droplet diameter (and with x_b replaced by the local quality at the spacer). Equation (3-22) would then be integrated from grid spacer to grid spacer (possibly in more than one step, depending on how quickly the wall heat flux varies) with initial conditions based on local conditions from the previous step.

CHAPTER VI

COMPARISON WITH OTHER MODELS AND PUBLISHED DATA

6.1 Dougall-Rohsenow

A large number of correlations of dispersed flow heat transfer can be found in the literature. Most of these are in the form of an effective heat transfer coefficient,

$$h = \frac{q_w''}{T_w - T_s} \quad . \tag{6-1}$$

Since this heat transfer coefficient is based on $T_w - T_s$ instead of $T_w - T_v$, the effect of vapor superheat is concealed within the heat transfer coefficient. These correlations should not, therefore, be used outside the region in which they are developed.

Perhaps the most widely used of all correlations is the Dougall-Rohsenow correlation [11], which is basically equivalent to an assumption of thermal equilibrium.

$$h_w = .023 \frac{k_v}{D_T} \, Pr_v^{.4} \left(\frac{G D_T x}{\mu_v \alpha_h} \right)^{.8} \tag{6-2}$$

Since all properties are evaluated at equilibrium temperature, it is to be expected that wall heat transfer coefficients will be overestimated and wall temperatures underestimated. It will be shown later in this

chapter, however, that even evaluating properties at film temperture will often result in underestimated wall temperatures.

Two other correlations, by Groeneveld and Delorme [10] and by Chen et al [9] are considered here, because they explicitly account for vapor superheating.

6.2 Groeneveld and Delorme

In Groeneveld and Delorme's correlation, vapor temperature and actual quality are found from

$$\frac{i_v - i_g}{i_{fg}} = \exp(-\tan\psi) \qquad (6\text{-}3)$$

$$= \frac{x_e}{x} - 1 \quad , \qquad (6\text{-}4)$$

where

$$\psi = .13864\ Pr_v^{.20}\ Re_h^{.20006} \left(\frac{q_w'' C_{pv} D_T}{k_v\ i_{fg}}\right)^{-.09232} (1.3072 - 1.0833\ x_e + .8455\ x_e^2) \quad , \qquad (6\text{-}5)$$

where

$$Re_h = \frac{G D_T}{\mu_v}\left(x_1 + \frac{\rho_v}{\rho_\ell}(1 - x_1)\right) \quad , \qquad (6\text{-}6)$$

where $x_1 = x_e$ for $0 \leq x_e \leq 1$, $x_1 = 1$ for $x_e > 1$, $\psi = 0$ for $\psi < 0$, and $\psi = \frac{\pi}{2}$ for $\psi > \frac{\pi}{2}$. In Equations (6-5) and (6-6), properties are evaluated at equilibrium temperature. Wall temperature is

then found using Hadaller's heat transfer correlation [28],

$$Nu_f = .008348\left(\frac{G D_T}{\mu_f}\left(x + \frac{\rho_v}{\rho_\ell}(1 - x)\right)\right)^{.8774} Pr_f^{.6112} \quad , \quad (6\text{-}7)$$

where properties are evaluated at film temperature.

6.3 Chen, et al

In the correlation of Chen et al, actual quality and vapor temperature are found, knowing wall temperature, by solving the two following equations simultaneously.

$$\frac{x_e}{x} = 1 + \frac{i_v - i_g}{i_{fg}} \quad , \text{ and} \quad (6\text{-}8)$$

$$\frac{x}{x_e} = 1 - \frac{.26}{1.15 - (p/p_{crit})^{.65}} \frac{T_v - T_s}{T_w - T_v} \quad , \quad (6\text{-}9)$$

where p_{crit} is the critical pressure. From these two equations, it is seen that, for a given pressure and wall temperature, there is a unique value of vapor temperature. Wall heat flux is then found using the wall heat transfer coefficient

$$h_w = .0185\ Gx\ Cp_f\ Pr_f^{-2/3}\left(\frac{G D_T}{\mu_{vf}}\left(x + \frac{\rho_v}{\rho_\ell}(1 - x)\right)\right)^{-.17} \quad ,$$

where, again, properties are evaluated at film temperature.

Clearly, this correlation is most easily applied when wall temperature is known, and Groeneveld and Delorme's correlation is more easily applied when wall heat flux is known. While both of these models account for vapor superheat explicitly, both models allow the vapor temperature to decrease as the flow travels down the tube, and both models allow the actual quality to drop below the dryout quality downstream of dryout. While the former phenomenon is not impossible (say, if droplet evaporation suddenly accelerated), it is contrary to the results of the present study. The latter phenomenon, on the other hand, is clearly impossible. These considerations aside, both correlations are reasonably successful in correlating the data from which they were developed.

6.4 Comparison with Data

In this section, the current model and the three other correlations are compared with seven sets of data by four authors. Four of these data sets are by Bennett et al [2], using water at 1000 psia. The fifth set is by Groeneveld [5], using Freon-12 at 160 psia. The sixth set is by Era et al [3] again using water at 1000 psia. The final set, by Hynek [1], uses nitrogen at 20 psia. These comparisons are plotted as $T_w - T_s$ against position downstream of dryout in Figures 6-1 through 6-7.

Bennet et al, Case I

In this case, shown in Figure 6-1, a large mass flux and small acceleration group combined to result in a small predicted value of the nonequilibrium parameter, K = .08. Despite the fact that this resulted in very little vapor superheat, the current model still somewhat overpredicts the data but, when properties are evaluated at film temperature, Dougall-Rohsenow virtually coincides with the current model. It is unlikely that evaluating properties at the film temperature per se resulted in an error in heat transfer coefficient. It is more likely that the presence of the droplets, especially this case with a low dryout quality, resulted in a larger heat transfer coefficient than was predicted. The results of Groeneveld and Delorme are not significantly different from those of the current model. It is notable that the results of Chen et al overpredict wall temperatures significantly,probably because vapor temperature is assumed to be a function of wall temperature alone.

Bennett et al, Case II

In this case, shown in Figure 6-2, the current model agrees with the data quite well, except near dryout, where entrance effects boost the wall heat transfer coefficient higher than predicted. Dougall-Rohsenow underpredicts wall temperatures badly, indicating that even a moderate amount of nonequilibrium (K = .22) results in significant wall temperature rises. Chen et al again overpredicts wall temperatures,

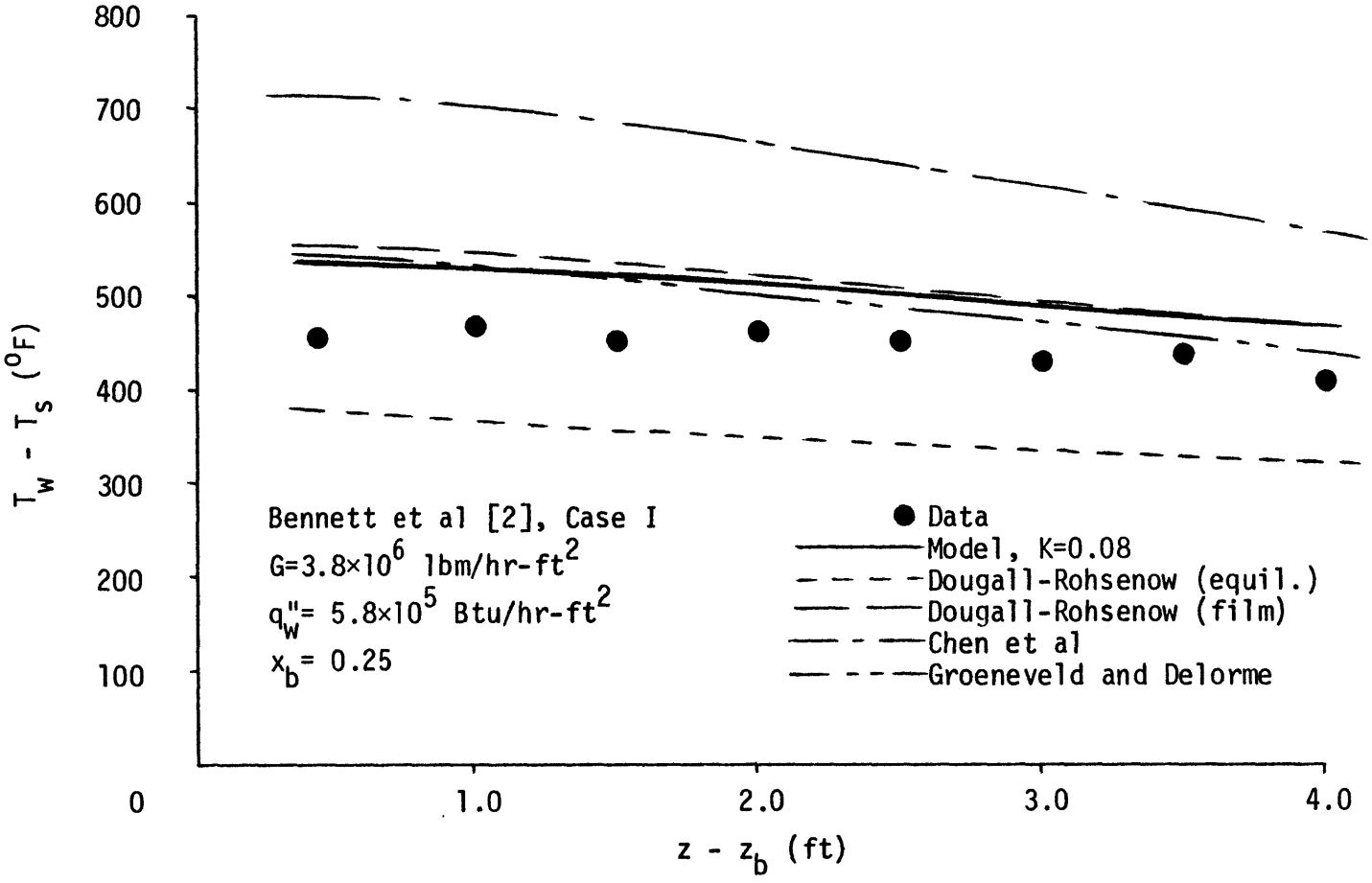

Figure 6-1. Comparison With Bennett et al, Case I

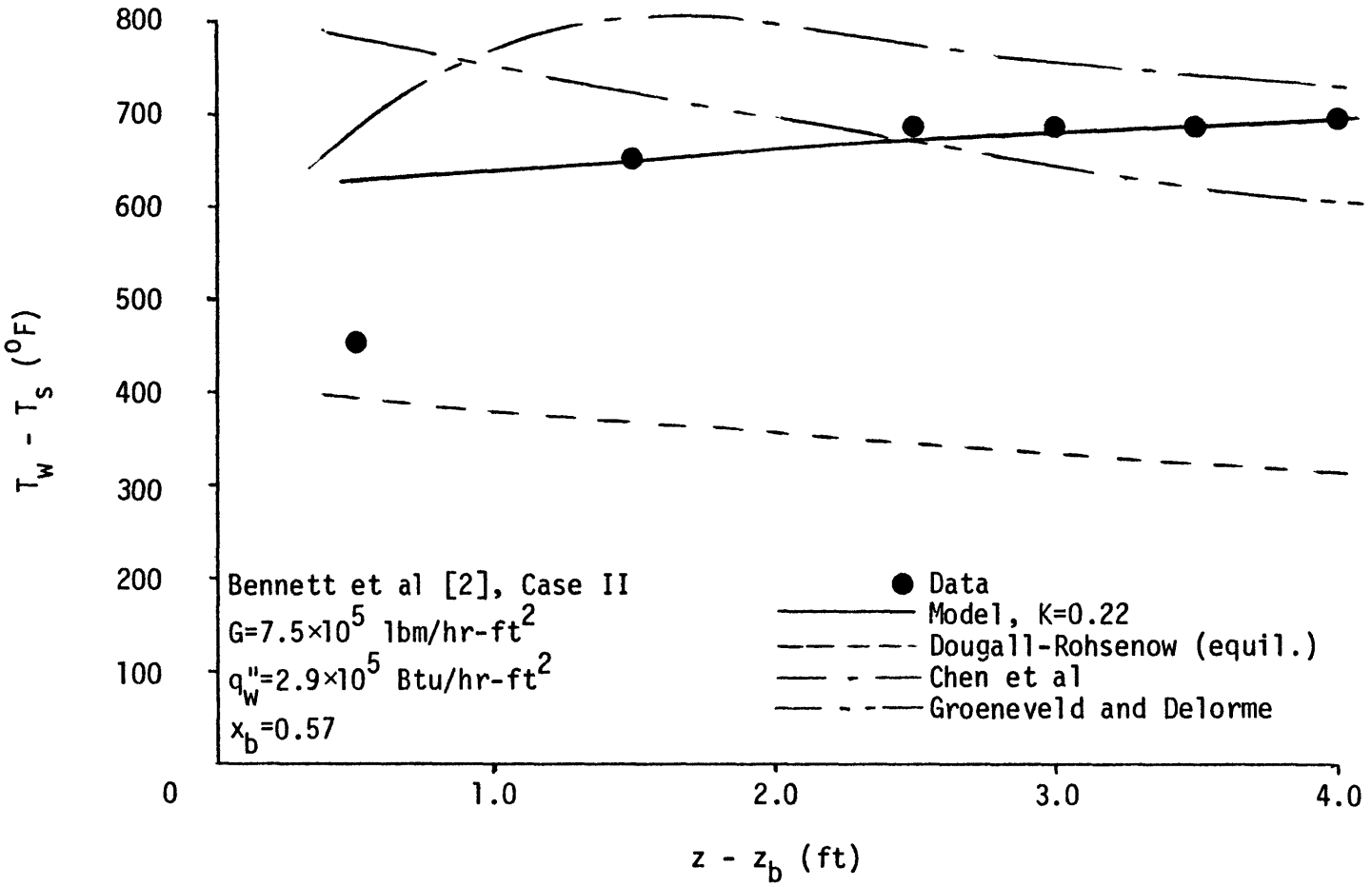

Figure 6-2. Comparison With Bennett et al, Case II

but indicates the right general trends with position. Groeneveld and Delorme, on the other hand, first overpredicts, then underpredicts the data, displaying the wrong trend. This is probably because the vapor temperature is predicted to decrease moving downstream.

Bennett et al, Case III

In this case, shown in Figure 6-3, a small mass flux and large acceleration group combine to result in a relatively large predicted value of the nonequilibrium constant, $K = .65$. The current model starts out well, but ends up overpredicting the wall temperature by roughly 80°F, possibly due to error in the wall heat transfer coefficient. In the meantime, Dougall-Rohsenow underpredicts wall temperatures badly, even when properties are evaluated at the film temperature. This is only to be expected, because of the high value of K. Groeneveld and Delorme again does not do well, again displaying the wrong trend with position. Chen et al starts off overpredicting wall temperature significantly, and ends up slightly underpredicting the data slightly. The current model is the only one that displays the right behavior.

Bennett et al, Case IV

In this case, shown in Figure 6-4, the current model underpredicts the data except near dryout, where entrance length effects are important. Dougall-Rohsenow badly underpredicts the wall temperatures once more. Chen et al again shows the proper behavior, but generally

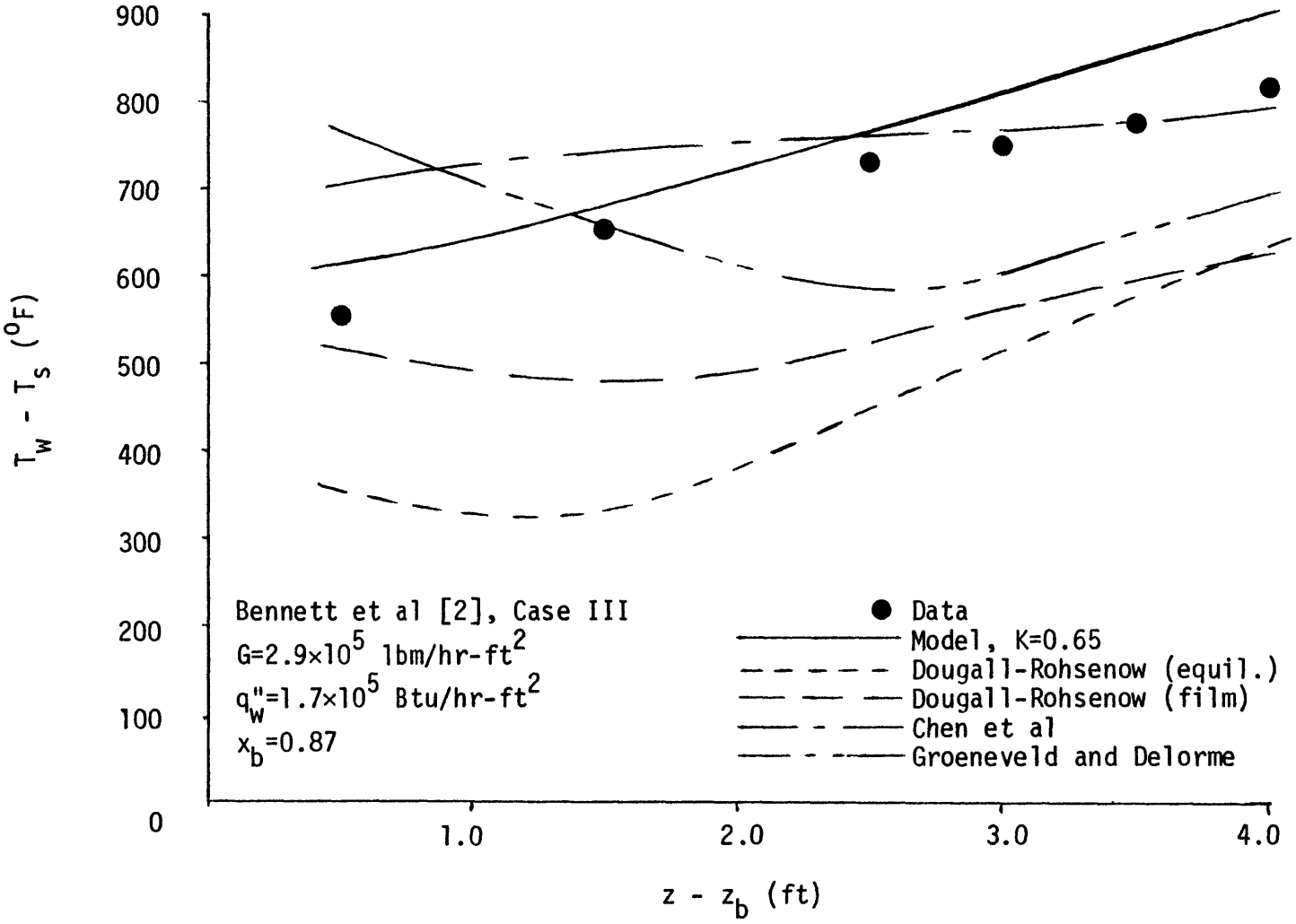

Figure 6-3. Comparison With Bennett et al, Case III

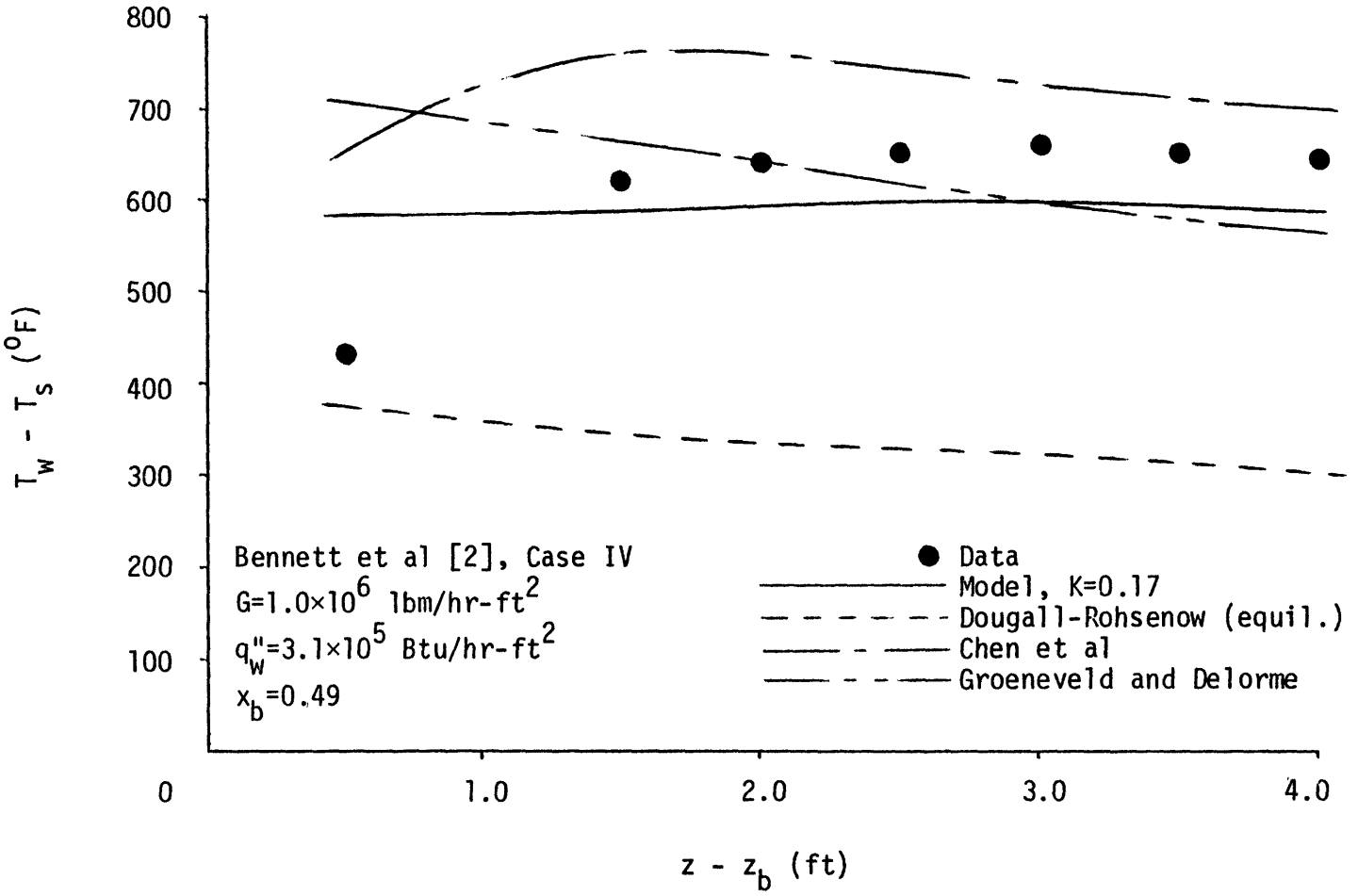

Figure 6-4. Comparison With Bennett et al, Case IV

overpredicts the wall temperatures more than the current model underpredicts them. Groeneveld and Delorme once more displays the wrong behavior with position.

In the four cases considered so far, the current model produces the best results overall. Chen et al generally displays the proper trend with position, but tends to overpredict wall temperature. Groeneveld and Delorme generally runs through the data, but displays the wrong trend with position. Dougall-Rohsenow runs a poor fourth.

Groeneveld

In this case, shown in Figure 6-5, all of the models display the right trend with position, with standout performances by the current model and, for once, Dougall-Rohsenow (evaluated at equilibrium temperature). Dougall-Rohsenow's good performance must be related to the low value of the nonequilibrium parameter, K = .10. Once again, Chen et al overpredicts the data, but not too badly, near the end. For once, Groeneveld and Delorme displays the right trend and does a reasonable job of predicting the data.

Era et al. and Hynek

In the case of Era et al , Figure 6-6, both Groeneveld and Delorme and Chen et al predict the data fairly well. This is not surprising, because both of these correlations were based, in part, on these data. It is also not surprising that, once again, Dougall-Rohsenow underpredicts the data.

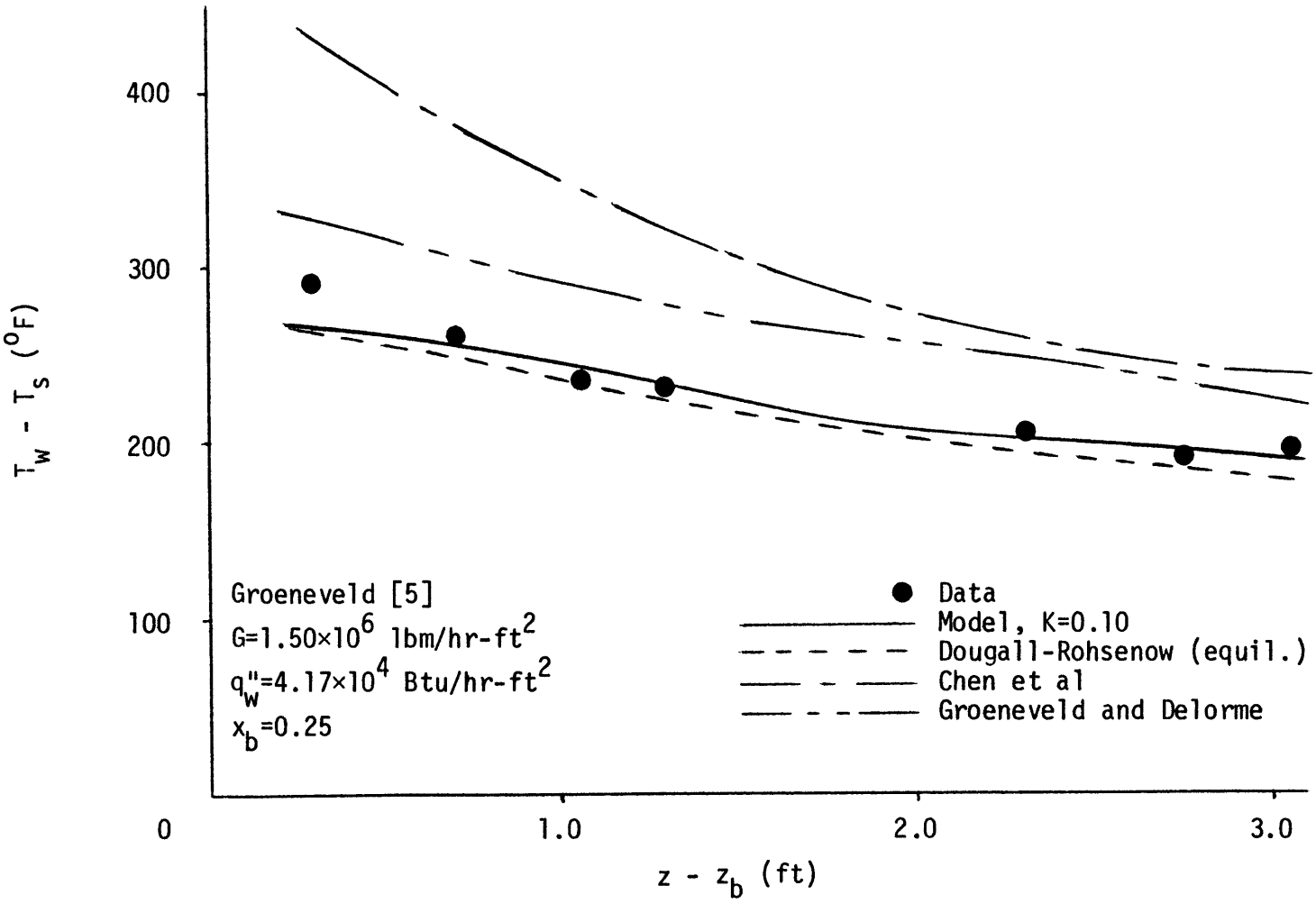

Figure 6-5. Comparison With Groeneveld [5]

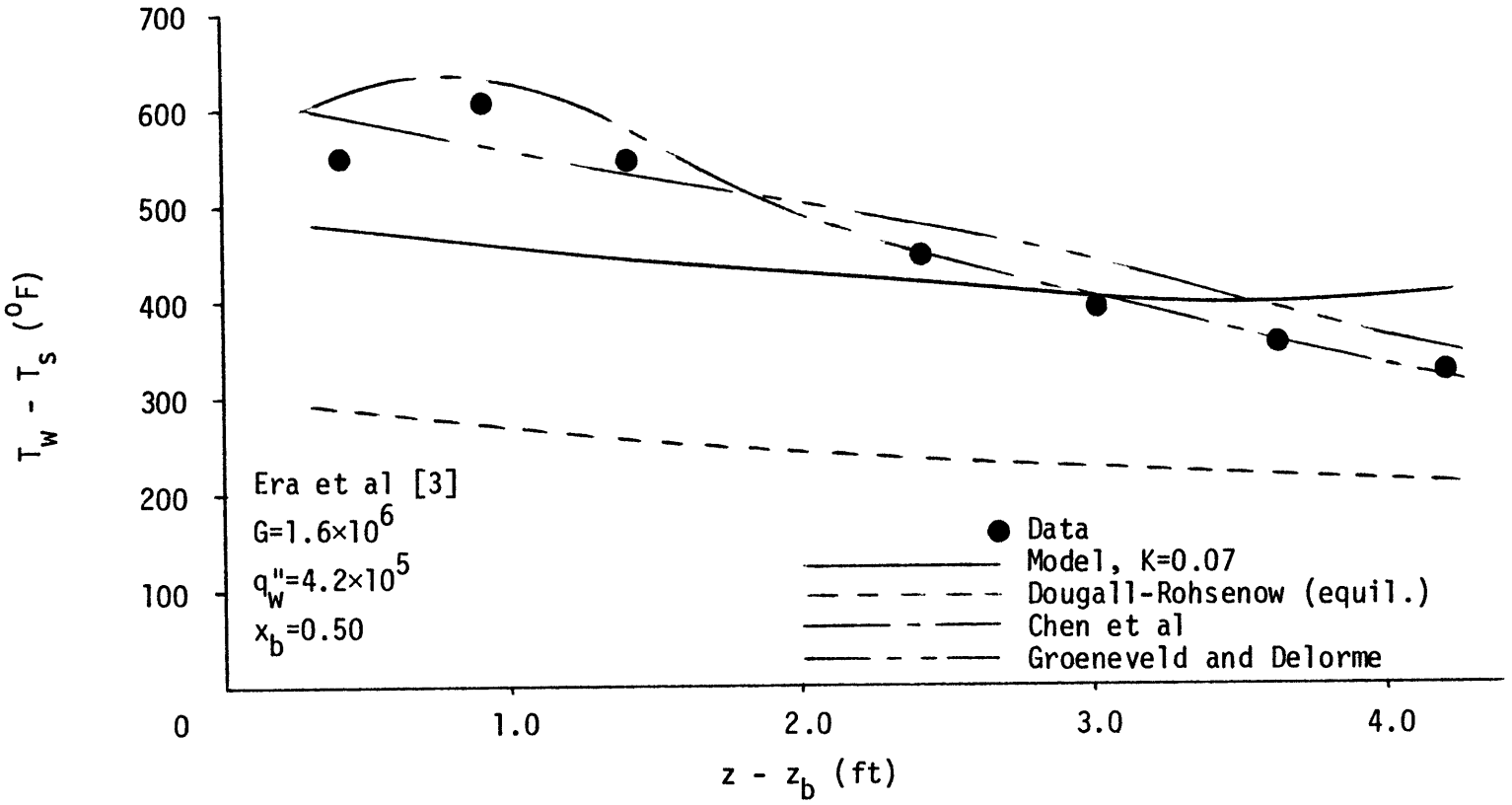

Figure 6-6. Comparison With Era et al [3]

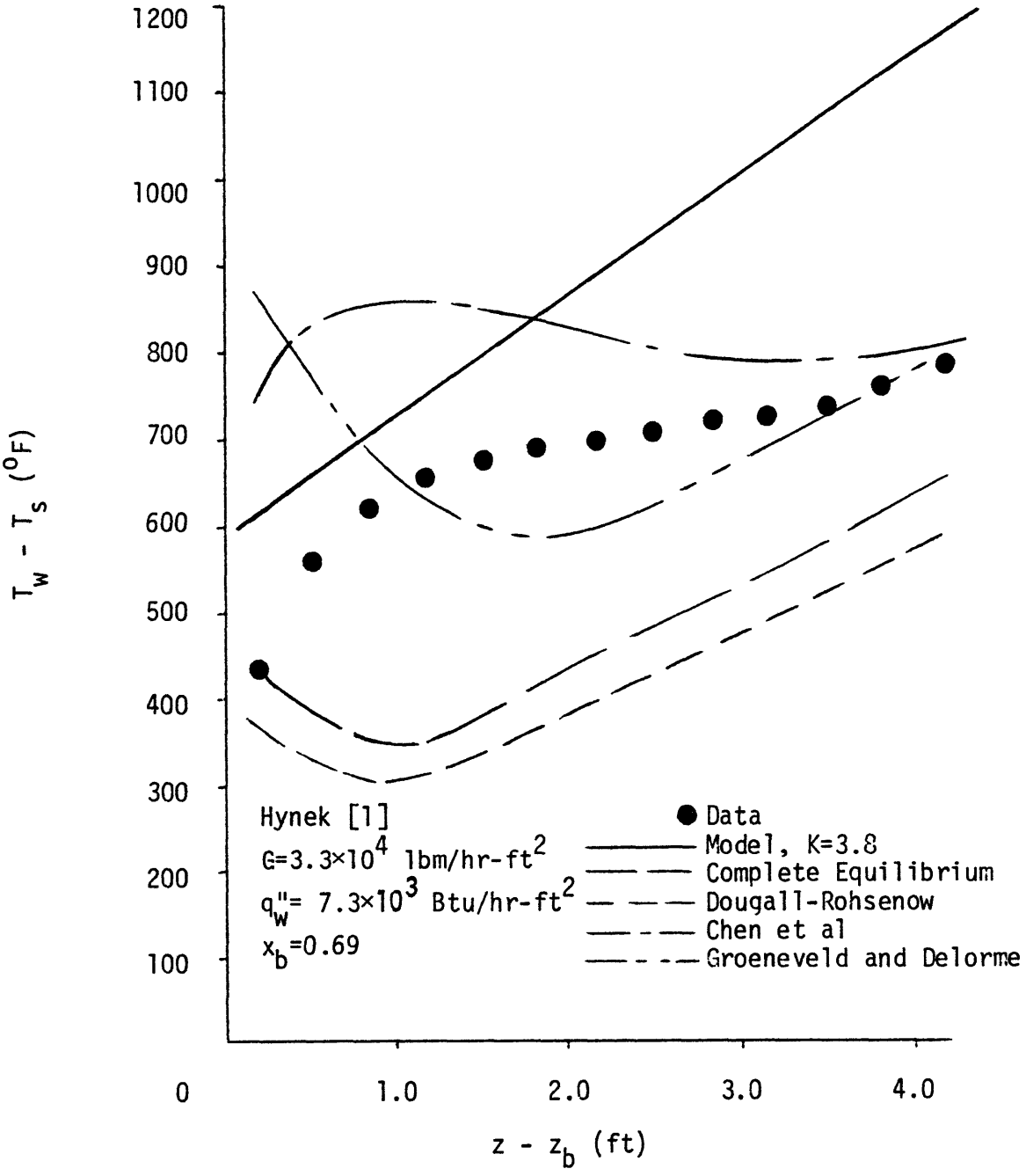

Figure 6-7. Comparison With Hynek [1]

In the case of Hynek, Figure 6-7, it is not surprising that neither Groeneveld and Delorme nor Chen et al predict the data well, because neither of these correlations was based on these data. It is again not surprising that Dougall-Rohsenow underpredicts the data.

What is surprising in both cases is how poorly the current model does at predicting the data. Both data sets display an apparent trend toward increasing equilibrium downstream of dryout, as if the value of K were decreasing. The present analysis indicates that, without droplet breakup, K should remain constant. Detailed calculations for these data sets show that free stream Weber numbers are very low; hence, droplet breakup should not occur to a significant extent. Therefore, the Local Conditions Solution cannot, in its present form, predict this behavior.

A possible explanation for this behavior is that free stream turbulence is enhancing the droplet heat transfer. The analysis of Calderbank and Moo-Young [29] predicts that, in the presence of strong turbulent fluctuations, and neglecting mass transfer shielding,

$$Nu_d \cong .058\left(\frac{GxD}{\mu_v \alpha_h}\right)^{.69} Pr_v^{1/3}$$

$$\sim x^{.69} \quad .$$

Comparing this result to Equation (3-15) where, neglecting mass transfer shielding, $Nu_d \sim x^{1/4}$, indicates that, if turbulent fluctuations (rather than droplet slip) do control droplet heat transfer, the value of K would appear to decrease downstream of dryout.

Further study is required to determine the following:

- Under what conditions one or the other of the two regimes of droplet heat transfer is controlling;
- A relation for the droplet Nusselt number when both regimes are important; and,
- The effect of the two regimes on wall temperature predictions.

6.5 Summary of Comparisons

In general, the current model compares well with the data of Bennett et al [2] and Groeneveld [5], with errors in $T_w - T_s$ being typically about 5%. The correlation of Chen et al [9] shows the right trends with position, but tends to overpredict wall temperatures. The correlation of Groeneveld and Delorme [10] does not display the right trends with position for the data of Bennet et al., but does predict the data of Groeneveld well. The Dougall-Rohsenow correlation only works for flows near equilibrium, and thus cannot be trusted in the general case.

An unexpected behavior is observed in the data of Era et al [3] and Hynek [1], in which there is an apparent trend toward increasing equilibrium downstream. A possible explanation of this behavior is that free stream turbulent fluctuations control droplet heat transfer in these data, so that more than one regime of the Local Conditions Solution may be necessary.

CHAPTER VII

SUMMARY

The Local Conditions Solution is a model of dispersed flow film boiling which, neglecting radiation and drop-wall interactions, yields a solution amenable to hand calculation. This model identifies a single nondimensional parameter which determines the extent of nonequilibrium in the flow. This nonequilibrium parameter requires the knowledge of conditions at dryout, particularly a characteristic droplet diameter.

Previously, no simple analytical model based on physical mechanisms occurring in annular flow had succeeded in predicting the droplet distribution at dryout. This is the purpose of this study.

The Local Conditions Solution is rederived including the behavior of a distribution of droplets. This rederivation results in the identification of the characteristic droplet diameter for purposes of dispersed flow heat transfer analysis.

The dryout droplet distribution is then derived. Coalescence and breakup of droplets in the free stream are neglected, leaving droplet entrainment and deposition as the controlling mechanisms. Existing correlations, modified where necessary to better model high pressure flows, are used for the individual mechanisms, eliminating the need for empirical constants.

Integration of the dryout droplet distribution results in a relatively simple method of calculating the characteristic droplet diameter. This characteristic droplet diameter is applied to the nonequilibrium parameter, resulting in a relatively simple, quickly applied solution technique.

The Local Conditions Solution is compared with three published correlations and published data from four investigators in water, Freon-12, and nitrogen. In five of seven cases examined, the current model gave results superior to those of the three published correlations, with errors in $T_w - T_s$ being typically about 5%. In the other two cases, the current model did not result in as good results, because the data displayed a trend toward increasing equilibrium downstream. The enhancement of droplet heat transfer by turbulent fluctuations may be the cause of this behavior.

CONCLUSIONS

1. The characteristic droplet diameter at dryout can be predicted relatively easily with the knowledge of flow parameters and dryout quality.
2. The Local Conditions Solution, with the characteristic droplet diameter model developed here, usually predicts wall temperatures which agree well with published wall temperature data.

3. Some published data display a trend toward increasing equilibrium downstream of dryout, contrary to predictions of the Local Conditions Solution.

RECOMMENDATIONS

Several areas which would benefit from further investigation can now be identified.

Information about droplet slip is lacking. A simple, accurate means of predicting the relative velocities between the vapor and droplets downstream of dryout is needed. This would allow more accurate estimation of droplet Nusselt and Weber numbers downstream of dryout.

Data on entrained droplet size and entrainment rate in heated and high pressure flows are needed. More accurate characterization of these mechanisms would allow a more accurate prediction of the distribution of droplet sizes at dryout.

To achieve direct verification of the droplet distribution model, the sizes of droplets entrained at dryout in heated flows should be measured experimentally.

Further study is needed into the relative effects of droplet slip and turbulent fluctuations on droplet heat transfer. This would allow the development of Local Conditions Solutions for more than one regime of droplet heat transfer.

APPENDIX I

ANNULAR FLOW MODEL

In this model, based on that of Wallis [13], the pressure gradients of the core and total flows are modeled separately, and equated to yield an additional interrelationship between the flow variables. In the following, vapor momentum losses due to droplet drag are neglected, as are droplet slip and the volume flow rate of the droplets ($\alpha_c \cong 1$).

A force balance on the core flow gives

$$-\frac{dp}{dz} - \rho_c g = \frac{4\tau_i}{D_T\sqrt{\alpha_f}} + \frac{4}{\pi D_T^2\,\alpha_f}\,\frac{d}{dz}\left[w_c V_c\right] , \qquad \text{(A1-1)}$$

where ρ_c is the average core density including droplets, τ_i is the interfacial shear, $D_T\sqrt{\alpha_f}$ is the average core diameter, and w_c and V_c are, respectively, core mass flow rate and average core velocity. Similarly, a force balance on the total flow yields

$$-\frac{dp}{dz} - \rho_c g = (1-\alpha_f)(\rho_\ell-\rho_c)g + \frac{4\tau_w}{D_T} + \frac{4}{\pi D_T^2}\,\frac{d}{dz}\left[w_f V_f + w_c V_c\right] , \qquad \text{(A1-2)}$$

where τ_w is the wall shear, and w_f and V_f are, respectively, film mass flow rate and average film velocity. The interface and wall shears are characterized by friction factors

$$\tau_i = \tfrac{1}{2} f_i \rho_c V_{rf}^2 , \qquad \text{(A1-3)}$$

and

$$\tau_w = \tfrac{1}{2} f_w \rho_\ell V_\ell^2 \quad . \tag{A1-4}$$

Wallis [13] characterized the interfacial friction factor as

$$f_i \cong .005[1 + 75(1 - \alpha_f)] \quad , \tag{A1-5}$$

and assumed a constant wall friction factor

$$f_w \cong .005 \quad . \tag{A1-6}$$

Neglecting droplet slip and droplet volume flow rate, the core density is approximately

$$\rho_c \cong \rho_v(1 + \frac{1-x}{x}\eta) \quad , \tag{A1-7}$$

where η is the entrainment fraction. The core velocity is then

$$V_c = \frac{G_c}{\rho_c \alpha_f} \cong \frac{Gx}{\rho_v \alpha_f} \quad . \tag{A1-8}$$

The film velocity is

$$V_f = \frac{G(1-x)(1-\eta)}{\rho_\ell(1-\alpha_f)} \quad , \tag{A1-9}$$

so the relative velocity between core and film is

$$V_{rf} \cong \frac{Gx}{\rho_v \alpha_f}\left(1 - \frac{\rho_v}{\rho_\ell}\,\frac{1-x}{x}\,\frac{\alpha_f}{1-\alpha_f}\,(1-\eta)\right) \quad . \tag{A1-10}$$

In this last equation, Wallis assumed a liquid surface velocity twice the average film velocity, but this resulted in numerical instabilities and multiple solutions in the resulting model. For this study, then, the liquid surface velocity was taken equal to the average film velocity. Identify from Eq. (2-10) that

$$dx = \frac{4A_c}{D_T}\,dz \quad . \tag{A1-11}$$

Equate dp/dz from Eqns. (A1-1) and (A1-2) and insert Eqns. (A1-3) through (A1-11) to obtain the following

$$\begin{aligned} 0 = {} & 10^{-2}\,\frac{x^2}{\alpha_f^{5/2}}\left(1 + 75(1-\alpha_f)\left(1 + \frac{1-x}{x}\,\eta\right)\left(1 - \frac{\rho_v}{\rho_\ell}\,\frac{1-x}{x}\,\frac{\alpha_f}{1-\alpha_f}\,(1-\eta)\right)^2\right. \\ & - \frac{D_T \rho_\ell \rho_v g}{G^2}\,(1-\alpha_f)\left(1 - \frac{\rho_v}{\rho_\ell}\left(1 + \frac{1-x}{x}\,\eta\right)\right) - 10^{-2}\,\frac{\rho_v}{\rho_\ell}\,\frac{(1-x)^2(1-\eta)^2}{(1-\alpha_f)^2} \\ & + \cdot 4A_c \left\{ \frac{1-\alpha_f}{\alpha_f}\left[\frac{2x}{\alpha_f}\left(1 + \frac{1-x}{x}\,\eta\right) - \frac{\eta}{\alpha_f}\right] + 2\,\frac{\rho_v}{\rho_\ell}\,\frac{(1-x)(1-\eta)^2}{(1-\alpha_f)}\right. \\ & - \frac{d\alpha_f}{dx}\left[\frac{1-\alpha_f}{\alpha_f^3}\,x^2\left(1 + \frac{1-x}{x}\,\eta\right) + \frac{\rho_v}{\rho_\ell}\,\frac{(1-x)^2(1-\eta)^3}{(1-\alpha_f)^2}\right] \\ & \left. + \frac{d\eta}{dx}\left[\frac{1-\alpha_f}{\alpha_f^2}\,x(1-x) + 2\,\frac{\rho_v}{\rho_\ell}\,\frac{(1-x)^2(1-\eta)}{1-\alpha_f}\right] \right\} \end{aligned} \tag{A1-12}$$

The bottom three lines of this equation account for acceleration, so including or ignoring these terms results in the accelerational or non-accelerational version of the model.

Because the entrainment fraction is not generally known as a function of position, some entrainment fraction profile must be assumed in order for a solution to be obtained. For purposes of this model, entrainment fraction was assumed to be characterized by

$$\eta = \tfrac{1}{2} \frac{x - x_0}{x_b - x_0} \left[1 + \frac{x - x_0}{x_b - x_0}\right] \quad , \qquad \text{(A1-13)}$$

where x_0 is the point at which entrainment is assumed to begin. This profile was chosen because it is simple and because it seems to fit the data of Hewitt et al, [27]. While the entrainment profile is probably a function of other flow parameters and properties, no conclusions can be drawn about the specific nature of this variation because insufficient data are available for heated flows. While Ishii and Grolmes [28] have developed a four part correlation for the initiation of entrainment, the results obtained using this correlation did not differ substantially from those obtained using an initial quality of 10%. Thus, using Eq. (A1-13) in Eq. (A1-12) with $x_0 = .10$, the annular flow model is complete.

The non-accelerational version of the model, the first two lines of Eq. (A1-12), is solved for film void fraction by the half-interval technique for different values of quality. The accelerational model is integrated from x_0 using a fourth-order Runge-Kutta algorithm. The initial void fraction used for the accelerational model was the void fraction predicted by the non-accelerational model at x_0.

Void fractions predicted by the two models generally agreed to within less than 1% error. Relative velocities between vapor and film calculated from these void fractions generally agreed to within 8%, with RMS errors of 6% being typical. Thus, for all intents and purposes, the results of the non-accelerational version of the annular flow model are equivalent to those of the accelerational version.

This model was used in the current study to verify the approximation

$$\alpha_f = \left(\frac{x}{x_b} \right)^{1/4} , \qquad (4\text{-}21)$$

to determine the behavior of V_{rf}/V_{fb} as a function of x/x_b, (Figure 4-1), and to derive the film slip ratio at dryout (Appendix II).

APPENDIX II

DRYOUT FILM SLIP RATIO AND RELATIVE VELOCITY

The film slip ratio is defined as

$$S_f \equiv \frac{V_c}{V_f} \quad . \tag{A2-1}$$

From Eqns. (A1-8) and (A1-9),

$$V_c \cong \frac{Gx}{\rho_v \alpha_f}$$

and

$$V_f \cong \frac{G(1-x)(1-\eta)}{(1-\alpha_f)} \quad .$$

Thus,

$$S_f \cong \frac{\rho_\ell}{\rho_v} \frac{x(1-\alpha_f)}{\alpha_f(1-x)(1-\eta)} \quad . \tag{A2-2}$$

Evaluating this expression at dryout, where α_f and η become unity, can be done using L'Hopital's rule, resulting in

$$S_{fb} \cong \frac{\rho_\ell}{\rho_v} \frac{x_b}{1-x_b} \left(\frac{\frac{d\alpha_f}{dx}}{\frac{d\eta}{dx}} \right)_b \quad . \tag{A2-3}$$

Evaluating the non-accelerational annular flow model (the first two lines of Eqn (A1-12)) at dryout similarly yields

$$x_b\left[1 - \frac{\rho_v}{\rho_\ell}\,\frac{1-x_b}{x_b}\left(\frac{\frac{d\eta}{dx}}{\frac{d\alpha_f}{dx}}\right)_b\right]^2 - \frac{\rho_v}{\rho_\ell}(1-x_b)^2\left(\frac{\frac{d\eta}{dx}}{\frac{d\alpha_f}{dx}}\right)_b^2 = 0 \quad . \qquad \text{(A2-4)}$$

Solving Eq. (A2-4) for $(d\eta/dx/d\alpha_f/dx)_b$ yields

$$\left(\frac{d\alpha_f/dx}{d\eta/dx}\right)_b = \frac{\left(1 - \frac{\rho_v}{\rho_\ell}\,\frac{1}{x_b}\right)(1-x_b)}{\sqrt{\frac{\rho_\ell}{\rho_b}\,x_b} - 1} \quad . \qquad \text{(A2-5)}$$

Combining Eqns. (A2-3) and (A2-5) results in

$$S_{fb} = \frac{\frac{\rho_\ell}{\rho_v}\,x_b - 1}{\sqrt{\frac{\rho_\ell}{\rho_v}\,x_b} - 1} \quad . \qquad \text{(A2-6)}$$

The relative velocity between the core and the film is

$$V_{rf} = V_c\left(1 - \frac{1}{S_f}\right) \quad . \qquad \text{(A2-7)}$$

At dryout, this gives

$$V_{rfb} = \frac{Gx_b}{\rho_v}\left(\frac{\frac{\rho_\ell}{\rho_v}\,x_b - 1 + 1 - \sqrt{\frac{\rho_\ell}{\rho_v}\,x_b}}{\frac{\rho_\ell}{\rho_v}\,x_b - 1}\right) \quad . \qquad \text{(A2-8)}$$

Cont'd.....

$$V_{rfb} = \frac{Gx_b}{\rho_v} \sqrt{\frac{\rho_\ell}{\rho_v} x_b} \frac{\sqrt{\frac{\rho_\ell}{\rho_v} x_b} - 1}{\frac{\rho_\ell}{\rho_v} x_b - 1} \qquad \text{(A2-8)}$$

$$= \frac{Gx_b}{\rho_v} \frac{\sqrt{\frac{\rho_\ell}{\rho_v} x_b}}{\sqrt{\frac{\rho_\ell}{\rho_v} x_b} + 1} \quad .$$

APPENDIX III

SAMPLE CALCULATION

For illustrative purposes, wall temperature is predicted as a function of position for the data of Bennett et al. [2], Case II, illustrated in Figure 6-2.

FLUID PROPERTIES: H_2O, 1000 psia

T_s = 545°F $\quad i_{fg}$ = 650 Btu/lbm $\quad \mu_v$ = .0458 lbm/hr-ft

ρ_v = 2.243 lbm/ft^3 $\quad \sigma$ = 5.15×10^5 lbm/hr $\quad \mu_\ell$ = .223 lbm/hr-ft

ρ_ℓ = 46.32 lbm/ft^3 $\quad Pr_v$ = 1.50

FLOW PARAMETERS:

D_T = .04142 ft

G = 7.5×10^5 lbm/hr-ft^2

q''_w = 2.9×10^5 Btu/hr-ft^2

x_b = .57

DIMENSIONLESS GROUPS:

$$Ac \equiv \frac{q''_w}{G\, i_{fg}} = 5.95\times10^{-4}$$

$$Re_b = \frac{GD_T}{\mu_v}\left(x_b + \frac{\rho_v}{\rho_\ell}(1-x_b)\right) = 4.01\times10^5$$

$$\lambda x_b = \frac{.0338\ x_b}{(Re_b)^{1/8} Ac} = 6.5$$

$$We_b = \frac{G^2 x_b^2\ D_T}{\rho_v \sigma} = 6.5\times10^3$$

NONEQUILIBRIUM PARAMETER:

From Figures 4-4 and 4-5, with We_b , λx_b , and x_b known,

$$f = 1.94 \ ,$$

$$\phi = 1.10 \ .$$

Then, from Eq. (5-1),

$$K = .0013\ \frac{f\phi A_c^{3/4}\ Pr_v^{2/3}\ Re_b^{4/3}\left(\sqrt{\frac{\rho_\ell}{\rho_v}}\ x_b + 1\right)^{5/2}}{We_b^{5/4}\ (1-x_b)^{5/12}\ x_b^{7/4}\ \left(\frac{\rho_\ell}{\rho_v}\right)^{1/12}}\left(\frac{\mu_v}{\mu_\ell}\right)^{5/6}$$

$$= .22$$

ACTUAL QUALITY:

From Eq. (5-3), the radius of curvature at dryout is

$$r_b = \frac{K\ x_b^{7/4}}{(1-x_b)^{7/12}} = .13 \ .$$

In Figure A3-1, the graphical construction for actual quality vs. equilibrium quality is shown. Because no curve has been drawn for K = .22, the tangent line is drawn in at the estimated location for the exact solution, shown as a dashed line. Equilibrium quality is found from

$$x_e = x_b + \frac{4Ac}{D_T} z \quad ,$$

and actual quality is found from the graph.

VAPOR TEMPERATURE:

Vapor temperature is found from

$$\frac{i_v - i_g}{i_{fg}} = \frac{x_e}{x} - 1 \quad ,$$

where i_v is the actual vapor enthalpy, i_g is the vapor enthalpy at saturation, and i_{fg} is the latent heat of vaporization.

WALL TEMPERATURE:

The wall temperature is found from

$$T_w - T_v = \frac{q''_w}{h_w} \quad ,$$

where h_w is found from Hadaller's heat transfer correlation [27],

$$h_w = .008348 \frac{k_{vf}}{DT} Pr_f^{.6112} \left(\frac{G D_T}{\mu_{vf}} \left(x + \frac{\rho_v}{\rho_\ell} (1-x)\right)\right)^{.8774} \quad .$$

The properties required to calculate the wall heat transfer coefficient must be evaluated at the film temperature,

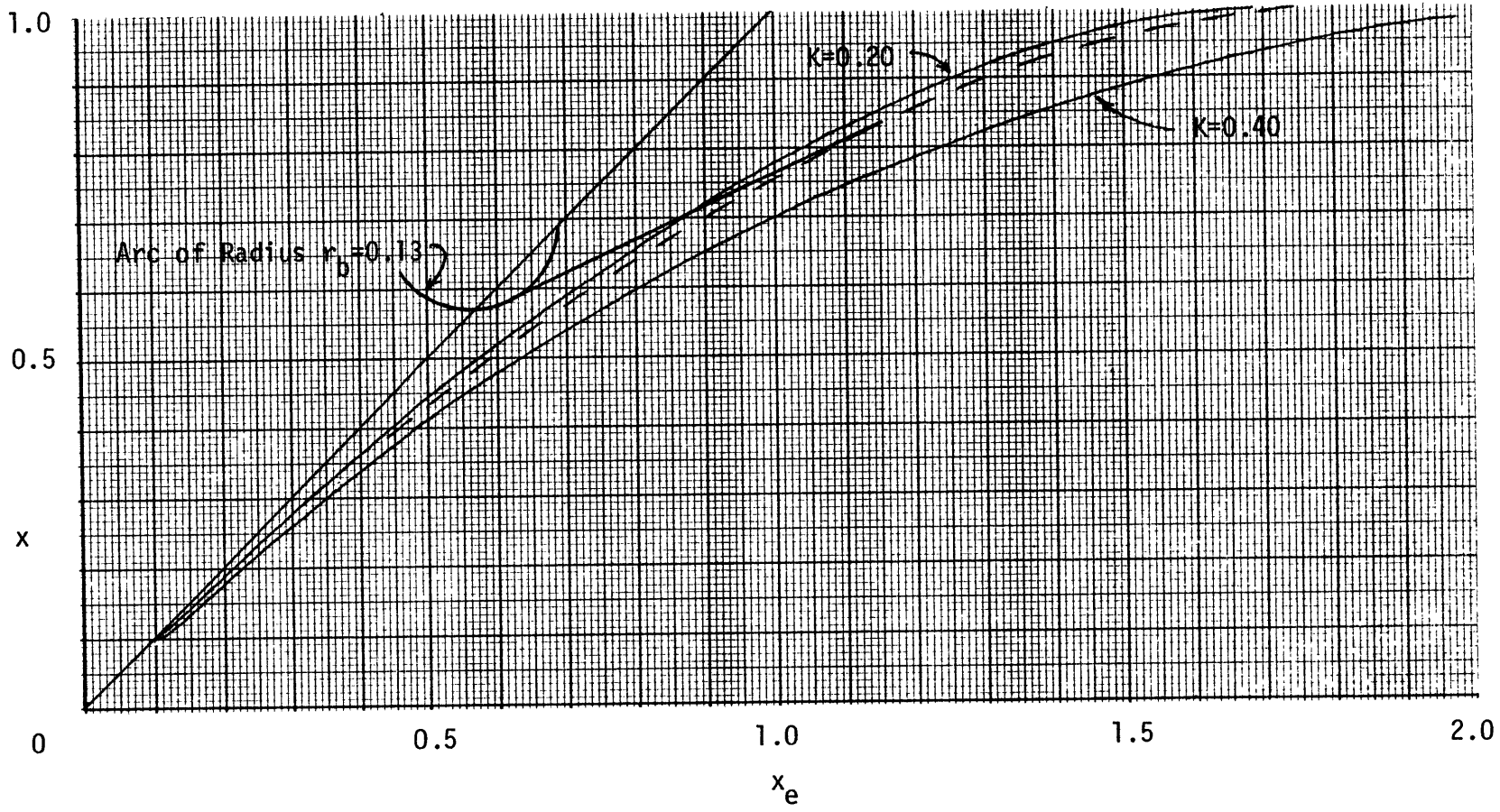

Figure A3-1. Actual Quality vs. Equilibrium Quality for Sample Calculation

$$T_f = \frac{1}{2}(T_v + T_w) \quad , \text{ which depends on } T_w .$$

Thus, in general, some iteration will be required to predict T_w. In the present case, however, the answer has already been provided, so no iteration is required unless the predicted wall temperatures differ significantly from the data.

This solution is summarized in Table A3-1, on the following page. For all points except the first, the predicted wall temperature is close enough to the actual (data) wall temperature that no iteration is necessary. Because the current model is not expected to do well very near dryout because of entrance effects, there is no point in iterating on the first data point either.

FROM DATA	$= x_b + 4A_c/D_T\, z$	FROM FIGURE A3-1		FROM $i_v = i_g + i_{fg}\left(\frac{x_e}{x} - 1\right)$	FROM DATA	$= \frac{1}{2}(T_v + T_w)$	BASED ON FILM TEMPERATURE	$= \frac{G\, D_T}{\mu_{vf}}\left(x + \frac{\rho_v}{\rho_\ell}(1-x)\right)$	$= .008348 \frac{k_{vf}}{D_T} Re_f^{.8774}\, Pr_{vf}^{.6112}$	$= \frac{q''_w}{h_w}$	$= T_v + (T_w - T_v)$
z(ft)	x_e	x	$\frac{x_e}{x} - 1$	T_v(°F)	T_w(°F)	T_f(°F)	Pr_{vf}	Re_f	$h_w\left(\frac{Btu}{hrft^2}\right)$	$T_w - T_v$(°F)	T_w(°F)
.5	.599	.573	.045	571	995	783	1.03	2.93×10^5	480	604	1175
1.5	.656	.603	.088	601	1195	898	.95	2.84×10^5	493	588	1189
2.5	.714	.629	.135	638	1232	935	.94	2.82×10^5	505	574	1213
3.0	.742	.642	.156	656	1229	943	.94	2.88×10^5	517	561	1217
3.5	.771	.655	.177	675	1230	953	.94	2.90×10^5	525	552	1228
4.0	.800	.668	.198	695	1237	966	.94	2.91×10^5	532	545	1240

TABLE A3-1. SUMMARY OF SAMPLE CALCULATION

REFERENCES

1. Hynek, S.J., "Forced Convection Dispersed Flow Film Boiling", Ph.D. Thesis, Massachusetts Institute of Technology, 1969.

2. Bennett, A.W., Hewitt, G.F., Kearsey, H.A., and Keeys, R.F.K., "Heat Transfer to Steam-Water Mixtures in Uniformly Heated Tubes in which the Critical Heat Flux has been Exceeded", AERE-R5373.

3. Era, A., Gaspari, G.P., Hassid, A., Milani, A., and Zavattarelli, R., "Heat Transfer Data in the Liquid Deficient Region for Steam-Water Mixtures at 70 kg/cm^2 Flowing in Tubular and Annular Conduits", CISE-R-184, 1966.

4. Forslund, R.P., "Thermal Non-Equilibrium in Dispersed Flow Film Boiling in a Vertical Tube", Ph.D. Thesis, Massachusetts Institute of Technology, December, 1966.

5. Groeneveld, D.C., "The Thermal Behavior of a Heated Surface at and Beyond Dryout", AECL-5309, November, 1972.

6. Cumo, M., Farello, G.E., and Ferrari, G., "The Influence of Curvature in Post-Dryout Heat Transfer", Report of the XXVI National ATI Annual Meeting, L'Aquila, September, 1971.

7. Koizumi, Y., Ueda, T., and Tanaka, H., "Post Dryout Heat Transfer to R-113 Upward Flow in a Vertical Tube", Int. J. of Heat and Mass Transfer, Vol. 22, pp. 669-678.

8. Groeneveld, D.C., and Gardner, S.R.M., "Post-CHF Heat Transfer under Forced Convective Conditions", AECL-5883.

9. Chen, J.C., Ozkaynak, F.T., and Sundaram, R.K., "Vapor Heat Transfer in Post-CHF Region Including the Effect of Thermal Non-Equilibrium", Nuclear Eng. and Design, Vol. 51, 1979, pp. 143-155.

10. Groeneveld, D.C., and Delorme, G.G.J., "Prediction of Thermal Non-Equilibrium in the Post-Dryout Regime", Nuclear Eng. and Design, Vol. 36, 1976, pp. 17-26.

11. Dougall, R.S., "Film Boiling on the Inside of Vertical Tubes with Upward Flow of the Fluid at Low Qualities", M.I.T. Heat Transfer Laboratory Report No. 9079-26, 1963.

12. Yoder, G.L., "Dispersed Flow Film Boiling", Ph.D. Thesis, Massachusetts Institute of Technology, 1980.

13. Wallis, G.B., "Annular Two Phase Flow" - "Part 1: A Simple Theory", and "Part 2: Additional Effects", J. Basic Eng., March, 1970, pp. 59-72, 73-82.

14. Ingebo, R.D., "Drag Coefficients for Droplets and Solid Spheres in Clouds Accelerating in Airstreams", NACA Technical Note 3762, September, 1956.

15. Ranz, W.E., and Marshall, W.R., Jr., "Evaporation from Drops", Parts I and II, Chemical Engineering Progress, Vol. 48, No. 3 and 4, 1952, pp. 141-146, 173-180.

16. Yuen, M.C., and Chen, L.W., "Heat Transfer Measurements of Evaporating Liquid Droplets", Int. J. of Heat and Mass Transfer, Vol. 21, 1978, pp. 537-542.

17. Hinze, J. O., "Fundamentals of the Hydrodynamic Mechanism of Splitting in Dispersion Processes", A.I.Ch.E. Journal, Vol. 1, No. 3, pp. 289-295.

18. Kataoka, I., Ishii, M., and Mishima, K., "Generation and Size Distribution of Droplet in Gas-Liquid Annular Two-Phase Flow", ANL/RAS/LWR 81-3.

19. Ahmad, S.Y., "Axial Distribution of Bulk Temperature and Void Fraction in a Heated Channel with Inlet Subcooling", Trans. ASME, Journal of Heat Transfer, November, 1970, pp. 595-609.

20. McCoy, D.D., and Hanratty, T.J., "Rate of Deposition of Droplets in Annular Two-Phase Flow", Int. J. of Multiphase Flow, Vol. 3, 1977, pp. 319-331.

21. Ishii, M., and Mishima, K., "Correlation for Liquid Entrainment in Annular Two-Phase Flow of Low Viscous Fluid", ANL/RAS/LWR 81-2, 1981.

22. Cousins, L.B., and Hewitt, G.F., "Liquid Phase Mass Transfer in Annular Two-Phase Flow: Droplet Deposition and Liquid Entrainment", AERE-R-5657, 1968.

23. Cumo, M., Ferrari, G., and Farello, G.E., "A Photographic Study of Two Phase Highly Dispersed Flow, CNEN RT/ING (71) 8.

24. Ueda, T., "Entrainment Rate and Size of Entrained Droplets in Annular Two Phase Flow", Bull. Japan Soc. Mech. Eng., Vol. 22, No. 171, September 1979, pp. 1258-1265.

25. Hull, L.M., "Thermal Boundary Layer Development in Dispersed Flow Film Boiling", Ph.D. Thesis, Massachusetts Institute of Technology, May, 1982.

26. Hadaller, G., and Banerjee, S., "Heat Transfer to Superheated Steam in Round Tubes", AECL unpublished report, 1969.

27. Hewitt, G.F., Kearsey, H.A., Lacey, P.M.C., and Pulling, D.J., "Burnout and Film Flow in the Evaporation of Water in Tubes", AERE-R-4864, 1965.

28. Ishii, M., and Grolmes, M.A., "Inception Criteria for Droplet Entrainment in Two Phase Concurrent Film Flow, AIChE Journal, Vol. 21, No. 2, pp.308-318.

29. Calderbank, P.H., and Moo-Young, M.B., "The Continuous Phase Heat and Mass Transfer Properties of Dispersions", Chem. Eng. Sci., Vol. 16, 1961, pp. 39-54.